Bulletin of Mathematical Biology (1998) **60**, 857–900
Article No. bu980042

Continuous and Discrete Mathematical Models of Tumor-induced Angiogenesis

A. R. A. ANDERSON AND M. A. J. CHAPLAIN
Department of Mathematics,
University of Dundee,
Dundee DD1 4HN,
U.K.

E-mail: sanderso@mcs.dundee.ac.uk
E-mail: chaplain@mcs.dundee.ac.uk

Angiogenesis, the formation of blood vessels from a pre-existing vasculature, is a process whereby capillary sprouts are formed in response to externally supplied chemical stimuli. The sprouts then grow and develop, driven initially by endothelial-cell migration, and organize themselves into a dendritic structure. Subsequent cell proliferation near the sprout tip permits further extension of the capillary and ultimately completes the process. Angiogenesis occurs during embryogenesis, wound healing, arthritis and during the growth of solid tumors. In this paper we present both continuous and discrete mathematical models which describe the formation of the capillary sprout network in response to chemical stimuli (tumor angiogenic factors, TAF) supplied by a solid tumor. The models also take into account essential endothelial cell–extracellular matrix interactions via the inclusion of the matrix macromolecule fibronectin. The continuous model consists of a system of nonlinear partial differential equations describing the initial migratory response of endothelial cells to the TAF and the fibronectin. Numerical simulations of the system, using parameter values based on experimental data, are presented and compared qualitatively with *in vivo* experiments. We then use a discretized form of the partial differential equations to develop a biased random-walk model which enables us to track individual endothelial cells at the sprout tips and incorporate anastomosis, mitosis and branching explicitly into the model. The theoretical capillary networks generated by computer simulations of the discrete model are compared with the morphology of capillary networks observed in *in vivo* experiments.

1. INTRODUCTION

Angiogenesis (*syn* neovascularization), the formation of blood vessels from a pre-existing vasculature, is a crucial component of many mammalian growth processes. It occurs in early embryogenesis during the formation of the placenta after implantation of the blastocyst in the uterine wall (Graham and Lala,

0092-8240/98/050857 + 44 $30.00/0

1992). It also occurs, in a controlled manner, in adult mammals during tissue repair (Arnold and West, 1991; Pettet *et al.*, 1996). By contrast, uncontrolled or excessive blood-vessel formation is essential for tumorigenesis and is also observed in arthritis, abnormal neovascularization of the eye, duodenal ulcers, and following myocardial infarction (Folkman, 1985, 1995; Folkman and Klagsbrun, 1987). These instances may be considered pathological examples of angiogenesis (Muthukkaruppan *et al.*, 1982; Folkman and Brem, 1992). In each case, however, the well-ordered sequence of events characterizing angiogenesis is the same, beginning with the rearrangement and migration of endothelial cells from a pre-existing vasculature and culminating in the formation of an extensive network, or bed, of new capillaries (Madri and Pratt, 1986).

The first event of tumor-induced angiogenesis involves the cancerous cells of a solid tumor secreting a number of chemicals, collectively known as tumor angiogenic factors (TAF) (Folkman and Klagsbrun, 1987), into the surrounding tissue. These factors diffuse through the tissue space creating a chemical gradient between the tumor and any existing vasculature. Upon reaching any neighboring blood vessels, endothelial cells lining these vessels are first induced to degrade the parent venule basement membranes and then migrate through the disrupted membrane towards the tumor. Several angiogenic factors, e.g., vascular endothelial growth factor (VEGF), acidic and basic fibroblast growth factor (aFGF, bFGF), angiogenin and others, have been isolated (Folkman and Klagsbrun, 1987; Relf *et al.*, 1997) and endothelial-cell receptors for these proteins have been discovered (Millauer *et al.*, 1993; Hatva *et al.*, 1995; Mandriota *et al.*, 1995; Fong *et al.*, 1995; Ortega and Plouet, 1995; Hewett and Murray, 1996; Ortega *et al.*, 1996; Patterson *et al.*, 1996; Duh *et al.*, 1997; Hanahan, 1997). Indeed, there is now clear experimental evidence that disrupting these receptors has a direct effect on the final structure of the capillary network (Dumont *et al.*, 1994; Fong *et al.*, 1995; Sato *et al.*, 1995; Hanahan, 1997).

The initial response of the endothelial cells to these angiogenic factors is a chemotactic one (Sholley *et al.*, 1984; Terranova *et al.*, 1985; Paweletz and Knierim, 1989; Stokes *et al.*, 1990), initiating the migration of the cells towards the tumor. Following this, small, finger-like capillary sprouts are formed by accumulation of endothelial cells which are recruited from the parent vessel. The sprouts grow in length due to the migration and further recruitment of endothelial cells (Cliff, 1963; Schoefl, 1963; Warren, 1966; Ausprunk and Folkman, 1977; Sholley *et al.*, 1984) and continue to move toward the tumor directed by the motion of the leading endothelial cell at the sprout tip. Further sprout extension occurs when some of the endothelial cells of the sprout wall begin to proliferate. Cell division is largely confined to a region just behind the cluster of mitotically inactive endothelial cells that constitute the sprout tip. This process of sprout tip migration and proliferation of sprout-wall cells forms solid strands of endothelial cells amongst the extracellular matrix. The cells continue to make their way through the extracellular matrix which consists of interstitial tissue,

collagen fiber and fibronectin as well as other components (Liotta *et al.*, 1983; Paweletz and Knierim, 1989). Interactions between the endothelial cells and the extracellular matrix are very important and directly affect cell migration. In particular, the specific interactions between the endothelial cells and fibronectin, a major component of the extracellular matrix, have been shown to enhance cell adhesion to the matrix.

Fibronectin is a matrix macromolecule which occurs in two distinctly different forms.

1. As a soluble glycoprotein found in various body fluids (including blood), known as plasma fibronectin.
2. As an insoluble constituent of the extracellular matrix and basement membranes of cells, known as cellular fibronectin (Hynes, 1990).

Cultured endothelial cells are known to synthesize and secrete cellular fibronectin (Birdwell *et al.*, 1978, 1980; Jaffee and Mosher, 1978; Macarak *et al.*, 1978; Rieder *et al.*, 1987; Sawada *et al.*, 1987) and the expression of this secreted fibronectin by the endothelial cells in cultures (*in vitro*) closely reflects the distribution of pre-existing fibronectin observed in matrices *in vivo* (Vlodavsky *et al.*, 1979; Hynes, 1990). The fibronectin which is produced and secreted by endothelial cells does not diffuse, but remains bound to the extracellular matrix (Birdwell *et al.*, 1980; Hynes, 1990), its central function being the adhesion of cells to the matrix (Schor *et al.*, 1981; Alessandri *et al.*, 1986). It is a major ligand (both cellular fibronectin and plasma fibronectin) between cells and matrix materials in many situations. Endothelial cells use fibronectin for attachment to the matrix via integrins, a family of cell-surface receptors (Johansson *et al.*, 1987; Hynes, 1990; Alberts *et al.*, 1994).

It has been verified experimentally that fibronectin stimulates directional migration of a number of cell types (including endothelial cells) in Boyden-chamber assays (Greenberg *et al.*, 1981; Goodman and Newgreen, 1985; Albini *et al.*, 1987; Woodley *et al.*, 1988). These results have demonstrated that fibronectin promotes cell migration up a concentration gradient and the results of Quigley *et al.* (1983), Lacovara *et al.* (1984) and McCarthy and Furcht (1984) have further demonstrated that this is a response of the cells to a gradient of adhesiveness of bound fibronectin, termed haptotaxis (Carter, 1965, 1967). Therefore, in addition to the chemotactic response of the endothelial cells to the TAF, there is a complementary haptotactic response to the fibronectin present within the extracellular matrix (Bowersox and Sorgente, 1982).

Initially, the sprouts arising from the parent vessel grow essentially parallel to each other. It is observed that once the finger-like capillary sprouts have reached a certain distance from the parent vessel, they tend to incline toward each other (Paweletz and Knierim, 1989), leading to numerous tip-to-tip and tip-to-sprout fusions known as anastomoses. Such anastomoses result in the fusing of the finger-like sprouts into a network of poorly perfused loops or arcades. Following

this process of anastomosis, the first signs of circulation can be recognized and from the primary loops, new buds and sprouts emerge repeating the angiogenic sequence of events and providing for the further extension of the new capillary bed. The production of new capillary sprouts from the sprout tips is often referred to as sprout branching, and as the sprouts approach the tumor, their branching dramatically increases until the tumor is eventually penetrated, resulting in vascularization (Muthukkaruppan *et al.*, 1982).

This process of repeated steps of endothelial-cell migration, sprout extension, cell proliferation and loop formation is necessary for the successful vascularization of the tumor. However, Sholley *et al.* (1984) demonstrated that, in the absence of endothelial-cell proliferation, a restricted capillary network, which stops after a few days and never reaches the tumor, is formed. Therefore, unless endothelial cells undergo mitosis, the capillary sprouts cannot complete vascularization successfully.

Tumor-induced angiogenesis provides the crucial link between the avascular phase of solid tumor growth and the more harmful vascular phase, wherein the tumor invades the surrounding host tissue and blood system (Chaplain, 1996). However, these apparently insidious features of tumor-induced angiogenesis are now being used to combat cancer growth and the clinical importance of angiogenesis as a prognostic tool is now well recognized (Harris *et al.*, 1994; Bikfalvi, 1995; Ellis and Fidler, 1995; Gasparini, 1995; Gasparini and Harris, 1995; Norton, 1995). Antiangiogenesis strategies are also being developed as a potentially powerful, non-invasive weapon against the spread of cancer (Herblin and Gross, 1994; Harris *et al.*, 1996; Harris, 1997).

In recent years several mathematical models, using different approaches, have been developed to describe some of the more important features of tumor-induced angiogenesis. Many of these models have used a continuum, deterministic framework in one space dimension (Liotta *et al.*, 1977; Zawicki *et al.*, 1981; Balding and McElwain, 1985; Chaplain and Stuart, 1993; Byrne and Chaplain, 1995; Orme and Chaplain, 1996). Although these models were capable of capturing some features of angiogenesis such as average sprout density and network expansion rates, they were unable to provide more detailed information concerning the actual structure and morphology of the capillary network and as such were of limited predictive value. More realistic continuum models of angiogenesis in two space dimensions have been considered by Chaplain (1995) and Orme and Chaplain (1997). The results of these models permit a more detailed qualitative comparison with *in vivo* observations concerning the spatiotemporal distribution of capillary sprouts within the network. However, even with these models, it is not possible to capture certain important events such as repeated sprout branching and hence the overall dendritic structure of the network. More general two-dimensional continuum branching models, with potential application to a wide number of problems, have been considered by Meinhardt (1976, 1982) and Edelstein-Keshet and Ermentrout (1989).

In contrast to the deterministic models, the model of Stokes and Lauffenburger (1991) used a discrete probabilistic framework in two space dimensions, based on stochastic differential equations. This approach had the advantage of enabling the motion of individual endothelial cells to be followed. Realistic capillary network structures were generated by incorporating rules for sprout branching and anastomosis. As parameters were estimated, as far as possible, from available experimental data, this permitted both qualitative and quantitative comparisons with *in vivo* networks to be made. Although the model incorporated random motility and chemotaxis as mechanisms for cell migration, no account was taken of interactions between the endothelial cells and the extracellular matrix. The model was also unable to reproduce the fact that there is an increased frequency of branching at the edge of the network as the capillary sprouts become closer to the tumor. This observed feature of tumor-induced angiogenesis has been described as the 'brush border' effect (Gimbrone *et al.*, 1974; Ausprunk and Folkman, 1977; Zawicki *et al.*, 1981; Muthukkaruppan *et al.*, 1982; Sholley *et al.*, 1984).

The model we will present in this paper utilizes a novel combination of the continuum and probabilistic approaches, combining the strengths of each approach. The mathematical model will focus on three very important variables involved in tumor-induced angiogenesis; namely, endothelial cells, TAF and fibronectin, each of which has a crucial role to play. In the first instance, using conservation laws and a continuum approach, we will derive a system of coupled nonlinear partial differential equations modeling the initial chemotactic response of the endothelial cells to TAF and the haptotactic response of the endothelial cells to fibronectin. In the continuum model we will not consider endothelial-cell proliferation. This models the experiments of Sholley *et al.*, (1984) where, although endothelial cells were irradiated to prevent mitosis occurring, a restricted capillary network did form. From a discretized form of these partial differential equations, a discrete biased random-walk model will be derived enabling the paths of individual endothelial cells located at the sprout tips, and hence the individual capillary sprouts, to be followed. The processes of sprout branching, anastomosis and cell proliferation will be incorporated in this discrete biased random-walk model.

The morphological events that are involved in new blood-vessel formation have been defined by studies of *in vivo* systems such as the chick chorioallantoic membrane (CAM), animal corneal models and *in vitro* examination of endothelial-cell migration and proliferation (Folkman and Haudenschild, 1980). The particular experimental system upon which we will base our mathematical model is that of the implant of a solid tumor in the cornea of a test animal (Gimbrone *et al.*, 1974; Muthukkaruppan *et al.*, 1982). Parameter values used in the model will be based, as far as possible, on estimates obtained from experimental observations.

The main aims of the model are to examine the relative importance of chemotaxis and haptotaxis in governing the migration of the endothelial cells, to examine capillary network formation with and without proliferation of endothelial cells, and to produce theoretical capillary network structures, from a model

based on sound physiological principles with realistic parameter values, which are morphologically similar to those observed *in vivo*. It is possible to analyze these computed structures for quantitative information such as network expansion rates, loop formation and overall network architecture. Therefore, from the continuous and discrete models, both qualitative and quantitative comparisons can be made with observations from the *in vivo* experimental system to validate the assumptions of the model.

2. THE CONTINUOUS MATHEMATICAL MODEL

We will base our mathematical model on the experimental system of Gimbrone *et al.* (1974), Muthukkaruppan *et al.* (1982), whereby a small solid tumor or fragment of tumor is implanted in the cornea of a test animal close to the limbal vessels of the eye which are lined with endothelial cells. Anderson and Chaplain (1997) considered a one-dimensional model for capillary network formation in the absence of endothelial-cell proliferation, and it is essentially a more general form of this model that we develop here. We denote the endothelial-cell density per unit area by n, the TAF concentration by c and the fibronectin concentration by f.

As already discussed in the introduction we assume that the motion of the endothelial cells (at or near a capillary sprout tip) is influenced by three factors: random motility (analogous to molecular diffusion), chemotaxis in response to TAF gradients (Terranova *et al.*, 1985; Stokes *et al.*, 1990, 1991); haptotaxis in response to fibronectin gradients (Schor *et al.*, 1981; Bowersox and Sorgente, 1982; Quigley *et al.*, 1983; Lacovara *et al.*, 1984; McCarthy and Furcht, 1984). To derive the partial differential equation governing endothelial-cell motion, we first consider the total cell flux and then use the conservation equation for cell density. The three contributions to the endothelial-cell flux $\boldsymbol{J}_n$, are given by,

$$\boldsymbol{J}_n = \boldsymbol{J}_{random} + \boldsymbol{J}_{chemo} + \boldsymbol{J}_{hapto}.$$

To describe the random motility of the endothelial cells at or near the sprout tips, we assume a flux of the form $\boldsymbol{J}_{random} = -D_n \nabla n$, where D_n is a positive constant, the cell random-motility coefficient. We take the chemotactic flux to be $\boldsymbol{J}_{chemo} = \chi(c) n \nabla c$, where $\chi(c)$ is a chemotactic function. In previous models of tumor-induced angiogenesis $\chi(c)$ is often assumed to be constant, meaning that endothelial cells always respond to a chemosensory stimulus (e.g., TAF) in the same manner, regardless of the stimulus concentration. We choose a receptor-kinetic law of the form

$$\chi(c) = \chi_0 \frac{k_1}{k_1 + c}, \tag{1}$$

reflecting the more realistic assumption that chemotactic sensitivity decreases with increased TAF concentration, where χ_0, the chemotactic coefficient, and k_1

are positive constants (Lapidus and Schiller, 1976; Lauffenburger *et al.*, 1984; Sherratt, 1994; Woodward *et al.* 1995; Olsen *et al.* 1997). The influence of fibronectin on the endothelial cells is modeled by the haptotactic flux, $\boldsymbol{J}_{hapto} = \rho_0 n \nabla f$, where $\rho_0 > 0$ is the (constant) haptotactic coefficient.

As we are focusing attention on the endothelial cells at the sprout tips (where there is no proliferation) and given that endothelial cells have a long half–life, in the order of months (Paweletz and Knierim, 1989), we omit any birth and death terms associated with the endothelial cells (we will consider endothelial-cell proliferation later in the section devoted to the discrete model). This also models the experiments of Sholley *et al.* (1984) where the cells were irradiated to stop proliferation, but the network formed to a certain extent.

The conservation equation for the endothelial-cell density n is therefore given by

$$\frac{\partial n}{\partial t} + \nabla \cdot \boldsymbol{J}_n = 0,$$

and hence the partial differential equation governing endothelial-cell motion (in the absence of cell proliferation) is,

$$\frac{\partial n}{\partial t} = D_n \nabla^2 n - \nabla \cdot (\chi(c) n \nabla c) - \nabla \cdot (\rho_0 n \nabla f)\,. \tag{2}$$

To derive the TAF equation, we first of all consider the initial event of tumor-induced angiogenesis which is the secretion of TAF by the tumor cells. Once secreted, TAF diffuses into the surrounding corneal tissue and extracellular matrix and sets up a concentration gradient between the tumor and any pre-existing vasculature such as the nearby limbal vessels. During this initial stage, where the TAF diffuses into the surrounding tissue (with some natural decay), we assume that the TAF concentration c satisfies an equation of the form:

$$\frac{\partial c}{\partial t} = D_c \nabla^2 c - \theta c \tag{3}$$

where D_c is the TAF diffusion coefficient and θ is the decay rate. We will assume that the steady-state of this equation establishes the TAF gradient between the tumor and the nearby vessels and provides us with the initial conditions for the TAF concentration profile. As the endothelial cells migrate through the extracellular matrix in response to this steady-state gradient (cf. Stokes and Lauffenburger, 1991), there is some uptake and binding of TAF by the cells (Ausprunk and Folkman, 1977; Hanahan, 1997). We model this process by a simple uptake function, resulting in the following equation for the TAF concentration:

$$\frac{\partial c}{\partial t} = -\lambda n c, \tag{4}$$

where λ is a positive constant, and the initial TAF concentration profile is obtained from the steady state of (3).

Fibronectin is known to be present in most mammalian tissue and has been identified as a component of the tissue of the cornea (Kohno *et al.*, 1983, 1987; Ben-Zvi *et al.*, 1986; Sramek *et al.*, 1987). In addition to this pre-existing fibronectin, it is known that the endothelial cells themselves produce and secrete fibronectin (Birdwell *et al.*, 1978, 1980; Jaffee and Mosher, 1978; Macarak *et al.*, 1978; Monaghan *et al.*, 1983; Rieder *et al.*, 1987; Sawada *et al.*, 1987) which then becomes bound to the extracellular matrix and does not diffuse (Birdwell *et al.*, 1980; Hynes, 1990). Therefore, the equation for fibronectin contains no diffusion term. There is also some uptake and binding of fibronectin to the endothelial cells as they migrate toward the tumor (Hynes, 1990). These production and uptake processes are modeled by the following equation:

$$\frac{\partial f}{\partial t} = \omega n - \mu n f, \tag{5}$$

where ω and μ are positive constants.

Hence the complete system of equations describing the interactions of the endothelial cells, TAF and fibronectin as detailed in the previous paragraphs is

$$\begin{aligned}
\frac{\partial n}{\partial t} &= \overbrace{D_n \nabla^2 n}^{\text{random motility}} - \overbrace{\nabla \cdot \left(\frac{\chi_0 k_1}{k_1 + c} n \nabla c \right)}^{\text{chemotaxis}} - \overbrace{\nabla \cdot (\rho_0 n \nabla f)}^{\text{haptotaxis}}, \\
\frac{\partial f}{\partial t} &= \overbrace{\omega n}^{\text{production}} - \overbrace{\mu n f}^{\text{uptake}}, \\
\frac{\partial c}{\partial t} &= - \overbrace{\lambda n c}^{\text{uptake}}.
\end{aligned} \tag{6}$$

This system is considered to hold on a square spatial domain of side L (representing a square of corneal tissue) with the parent vessel (e.g., limbal vessel) located along one edge and the tumor located on the opposite edge. We assume that the cells, and consequently the capillary sprouts, remain within the domain of tissue under consideration and therefore no-flux boundary conditions of the form

$$\underline{\zeta} \cdot (-D_n \nabla n + n (\chi(c) \nabla c + \rho_0 \nabla f)) = 0, \tag{7}$$

are imposed on the boundaries of the square, where $\underline{\zeta}$ is an appropriate outward unit normal vector.

We now nondimensionalize (6) by rescaling distance with the parent vessel to tumor distance of L, time with $\tau = L^2/D_c$ (where D_c is the TAF diffusion coefficient), endothelial-cell density with n_0, and TAF and fibronectin concentration with c_0 and f_0 respectively (where n_0, c_0, f_0 are appropriate reference variables).

Therefore setting

$$\tilde{c} = \frac{c}{c_0}, \quad \tilde{f} = \frac{f}{f_0}, \quad \tilde{n} = \frac{n}{n_0}, \quad \tilde{t} = \frac{t}{\tau}$$

and dropping the tildes for clarity, we obtain the nondimensional system,

$$\begin{aligned}
\frac{\partial n}{\partial t} &= D\nabla^2 n - \nabla \cdot \left(\frac{\chi}{1+\alpha c} n \nabla c \right) - \nabla \cdot (\rho n \nabla f), \\
\frac{\partial f}{\partial t} &= \beta n - \gamma n f, \\
\frac{\partial c}{\partial t} &= -\eta n c,
\end{aligned} \tag{8}$$

where

$$D = \frac{D_n}{D_c}, \quad \chi = \frac{\chi_0 c_0}{D_c}, \quad \alpha = \frac{c_0}{k_1}, \quad \rho = \frac{\rho_0 f_0}{D_c},$$
$$\beta = \frac{\omega L^2 n_0}{f_0 D_c}, \quad \gamma = \frac{\mu L^2 n_0}{D_c}, \quad \eta = \frac{\lambda L^2 n_0}{D_c},$$

and subject to the no-flux conditions,

$$\underline{\zeta} \cdot \left(-D\nabla n + n \left(\frac{\chi}{1+\alpha c} \nabla c + \rho \nabla f \right) \right) = 0 \tag{9}$$

on the boundaries of the unit square.

Wherever possible, parameter values have been estimated from available experimental data. An average distance from a tumor implant to parent vessels in the cornea is between 1 and 2 mm (Gimbrone *et al.*, 1974; Muthukkaruppan *et al.*, 1982) and we take the lengthscale $L = 2$ mm (cf. Stokes and Lauffenburger, 1991). The experiments of Stokes *et al.* (1990) and Rupnick *et al.* (1988) on endothelial-cell migration in response to angiogenic factors provide us with estimates for D_n, χ_0 and c_0. Endothelial-cell random motility coefficients in the range 2×10^{-9}–10^{-8} cm^2 s^{-1} were obtained. However, this was under the assumption that the cells moved independently. Rupnick *et al.* (1988) showed that when the movement of individual endothelial cells is constrained by surrounding cells, their estimate of the random motility coefficient was too large and did not agree with the experimental results. The formation of capillary sprouts causes a dependence on neighboring cells due to the formation of vessel walls—the endothelial cells which line the sprout wall are contiguous with one another. Therefore, one might expect a smaller random-motility coefficient than that observed by Rupnick *et al.* (1988), and we therefore take $D_n = 10^{-10}$ cm^2 s^{-1} (cf.

Bray, 1992). Other *in vivo* experimental results also indicate that there appears to be very little random motility of endothelial cells at the capillary sprout tips (Paweletz and Knierim, 1989; Paku and Paweletz, 1991). Stokes *et al.* (1990) measured the chemotactic coefficient of migrating endothelial cells in gradients of aFGF. The maximum chemotactic response was measured in concentrations of aFGF around 10^{-10} M giving a chemotactic coefficient of 2600 cm^2 s^{-1} M^{-1} and therefore we take $\chi_0 = 2600$ cm^2 s^{-1} M^{-1}, $c_0 \approx 10^{-10}$ M. In the absence of any available data for the haptotactic coefficient ρ_0, we assume that this is of the same magnitude as χ_0. As the endothelial cells generally migrate towards the tumor, even in the absence of proliferation, it is reasonable to assume that $\chi_0 > \rho_0$. Terranova *et al.* (1985) found that endothelial cells responded in a haptotactic manner to fibronectin in concentrations of fibronectin around 10^{-10} M and we take this as an estimate for f_0. Estimates for the diffusion coefficient of TAF are in the range 5×10^{-7}–5.9×10^{-6} cm^2 s^{-1} (Sherratt and Murray, 1990; Bray, 1992) and for our simulations, we take $D_c = 2.9 \times 10^{-7}$ cm^2 s^{-1}. Estimates of the parameters ω, μ, λ were not available since these are very difficult to obtain experimentally (Hynes, 1990).

These parameter values now give nondimensional values of $D = 0.00035$, $\chi = 0.38$ and we use a nondimensional value of $\rho = 0.34$. The estimates for L and D_c now give the timescale $\tau = L^2/D_c$ as 1.5 days.

The first event of tumor-induced angiogenesis is the secretion of TAF by the tumor cells. The TAF then diffuses into the extracellular matrix and a concentration gradient is established between the tumor and parent vessel. If we consider the tumor as approximately circular and model TAF diffusion using (3) then an approximation of the steady-state solution for such an equation (Chaplain, 1995, 1996) has a concentration field of the form,

$$c(x, y, 0) = \begin{cases} 1, & 0 \leq r \leq 0.1, \\ \dfrac{(\nu - r)^2}{\nu - 0.1}, & 0.1 \leq r \leq 1, \end{cases} \tag{10}$$

where ν is a positive constant and r is given by,

$$r = \sqrt{(x-1)^2 + \left(y - \tfrac{1}{2}\right)^2}, \tag{11}$$

assuming that the tumor is centered on $(1, \frac{1}{2})$, with a radius of 0.1. Taking (10) as the initial conditions for the TAF concentration profile might then be a reasonable description of the actual concentration field arising from a small circular tumor implant. To approximate a row of tumor cells (or a larger circular implant) we also consider an initial TAF concentration field of the form,

$$c(x, y, 0) = e^{-\frac{(1-x)^2}{\epsilon_1}}, \quad (x, y) \in [0, 1] \times [0, 1], \tag{12}$$

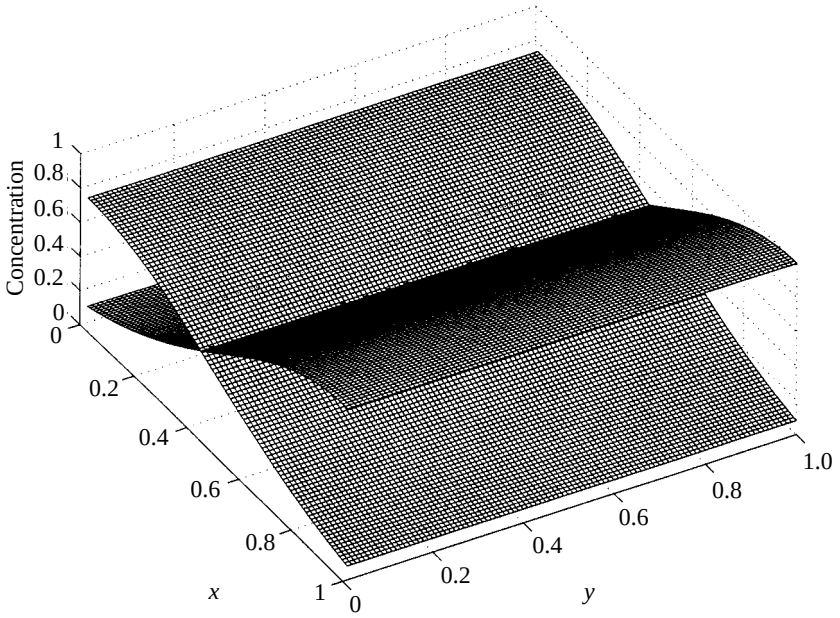

Figure 1. Initial fibronectin concentration (maximum value at $x = 0$) and initial TAF concentration (maximum value at $x = 1$) profiles for the two-dimensional simulations; $\epsilon_1 = \epsilon_2 = 0.45; k = 0.75$. The TAF concentration profile approximates a gradient produced by a line of tumour cells situated at $x = 1$. The fibronectin initial concentration is highest near the parent vessel at $x = 0$.

where ϵ_1 is a positive constant. In the simulations of the following sections using initial condition (12) emphasizes that any lateral motion of the endothelial cells is due to the interactions with TAF and fibronectin and is not dependent on the underlying geometry of the system.

Once the endothelial cells have been activated by TAF, they degrade their basal lamina leading to the damaging, and perhaps rupturing, of the parent-vessel basement membrane. This initial damage results in an increased vessel permeability (Clark *et al.*, 1981) which allows plasma fibronectin from the blood to leak from the parent vessel and diffuse into the corneal tissue (Hynes, 1990) [the diffusion coefficient of plasma fibronectin has been estimated at around 2×10^{-7} cm^2 s^{-1}, Williams *et al.* (1982) and Rocco *et al.* (1987)]. Subsequently, this plasma fibronectin becomes bound to the extracellular matrix of the corneal tissue (Oh *et al.*, 1981; Deno *et al.*, 1983; Clark *et al.*, 1983), creating a high initial concentration of fibronectin in and around the parent vessel. This has been observed experimentally by Clark *et al.* (1981, 1982, 1983) and Paku and Paweletz (1991). It has also been observed experimentally that high levels of laminin (another matrix macromolecule with similar adhesive properties to fibronectin) are initially found around the parent vessel (Hynes, 1990; Paku and Paweletz, 1991). In addition to this plasma fibronectin, there is also pre-existing cellular fibronectin distributed throughout the corneal tissue. We therefore take the initial concentration profile of fibronectin in the extracellular

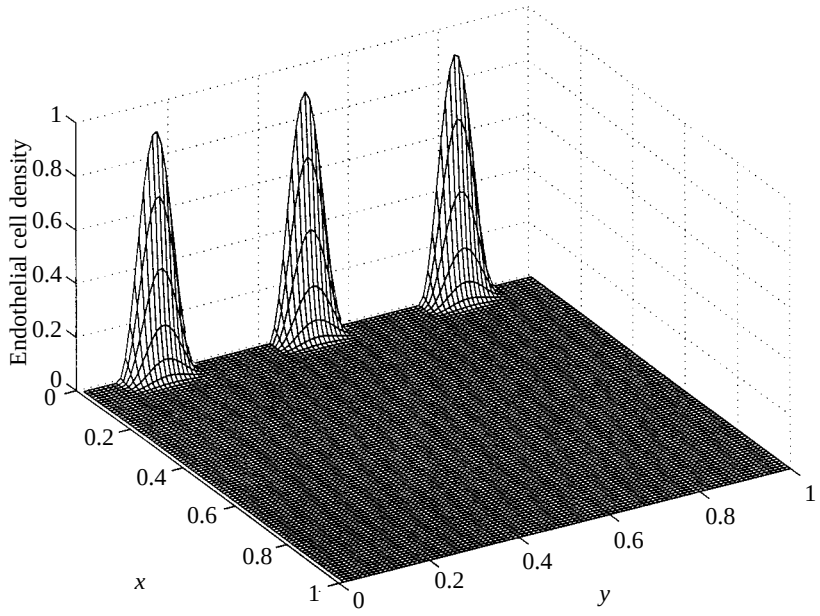

Figure 2. Initial endothelial-cell density distribution for the two-dimensional simulations representing the three initial regions of capillary sprout outgrowth; $\epsilon_3 = 0.001$.

matrix to have the form,

$$f(x, y, 0) = ke^{-\frac{x^2}{\epsilon_2}}, \quad (x, y) \in [0, 1] \times [0, 1]. \tag{13}$$

where $k < 1, \epsilon_2$ are positive constants. In other simulations, we also choose an initial spatially homogeneous fibronectin concentration representing the distribution of only pre-existing fibronectin in the extracellular matrix. Figure 1 contains a plot of the two-dimensional initial data for both the linear source TAF (12) and fibronectin (13). Parameters ϵ_1 and ϵ_2 were taken to be 0.45, and k was taken to be 0.75.

After the TAF has reached the parent blood vessel, the endothelial cells within the vessel form into a few cell clusters (Muthukkaruppan *et al.*, 1982; Orme and Chaplain, 1996) which eventually become sprouts. For simplicity, we will assume that initially three clusters form along the y-axis at $x \approx 0$, with the tumor located at $x = 1$ and the parent vessel of the endothelial cells at $x = 0$. The initial data is given by the distribution in Figure 2, which has three discrete peaks of the form $e^{-\frac{x^2}{\epsilon_3}} \sin^2(6\pi y)$, with the positive parameter $\epsilon_3 = 0.001$.

3. Two-dimensional Numerical Simulations

All of the numerical solutions presented in this section were obtained from a finite difference approximation of the system (8) with boundary and initial

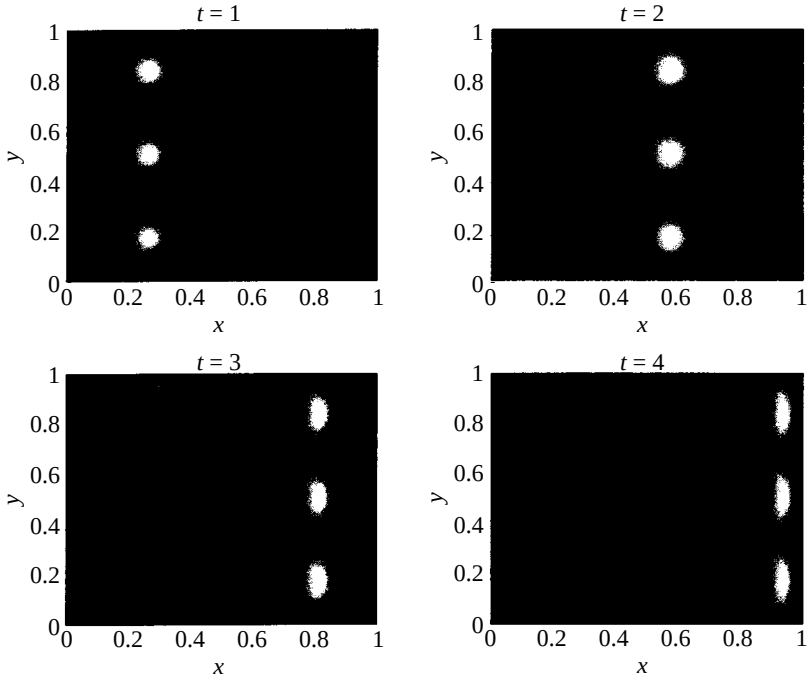

Figure 3. Spatiotemporal evolution of the endothelial-cell density from a numerical simulation of system (8) representing endothelial-cell migration from the parent vessel toward a line source of tumor cells without haptotaxis (see text for parameter values). The figure shows that the motion is almost entirely governed by chemotaxis with very little lateral movement. The three regions of cell density remain unconnected throughout the domain. The color graduation is directly proportional to the cell density, i.e., white is high density and black low density.

conditions (9)–(13). As there are no birth and death terms in the endothelial-cell equation (8) and we impose zero flux boundary conditions (9) then the total cell number is conserved. We used the conservation of cell number as a check on the accuracy of our numerical scheme which was found to be accurate to within 0.01%. The parameter values used in the simulations (unless specified otherwise) were $D = 0.00035$, $\chi = 0.38$, $\rho = 0.34$, $\eta = 0.1$, $\beta = 0.05$ and $\gamma = 0.1$.

In order to examine the relative importance of chemotaxis and haptotaxis in the model, we first of all consider the system in the absence of any haptotaxis (i.e., $\rho = 0$). With all other parameter values as above, data were obtained from our two-dimensional numerical code for four different times, producing the plots given in Fig. 3. We note that by $t = 2$ (3 days) the endothelial cells are more than half way through the domain, and by $t = 4$ (6 days) they have migrated almost completely across the domain. It is also important to note that there is very little lateral migration (i.e., movement parallel to the y-axis) of the endothelial cells. The bulk of the endothelial-cell density retains the shape of the initial distribution of the three peaks. This is because the motion is largely governed by chemotaxis with the small amount of lateral movement due to random motility.

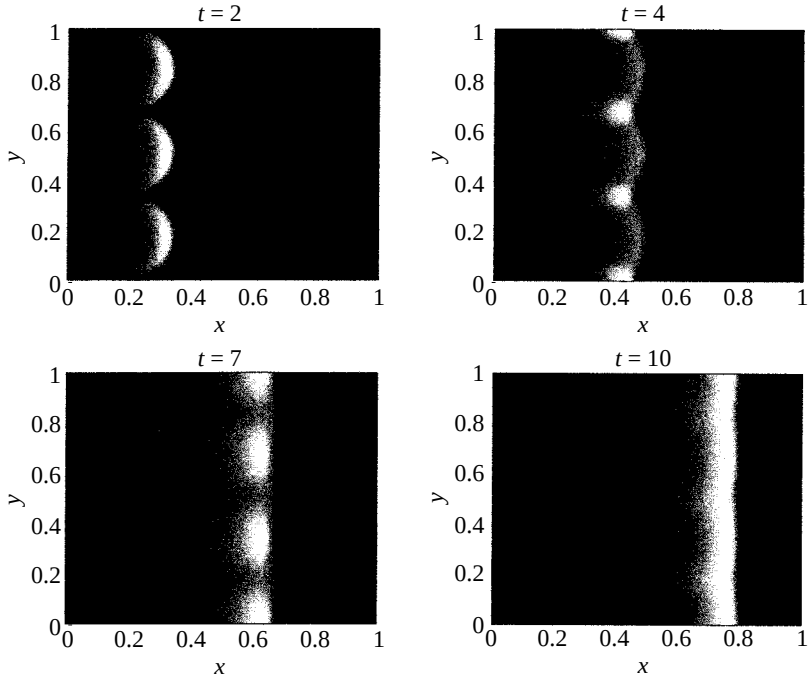

Figure 4. Spatiotemporal evolution of endothelial-cell density from a numerical simulation of system (8) representing endothelial-cell migration from the parent vessel toward a line source of tumor cells with both chemotaxis and haptotaxis (see text for parameter values). The effect that fibronectin and haptotaxis have on the endothelial cells is now apparent. The initial three regions of high cell density are drawn towards each other and first form a looped structure and then a band of high cell density. The color graduation is as in Fig. 3.

If we now include the effect of haptotaxis in the model, i.e., $\rho = 0.34$ (all other parameters having the same value as for Fig. 3), we obtain the four plots shown in Fig. 4. Comparing the plot at $t = 2$ (3 days) with that in Fig. 3, we see that cell migration towards the tumor is now slower and that the endothelial-cell density distribution is not as circular as in Fig. 3. The cell density distribution in each cluster appears as a crescent-like shape. This is due to the lateral migration of the endothelial-cell clusters towards one another. By $t = 4$ (6 days) we see that the three separate clusters have joined to form a continuous band of cell density. At $t = 7$ (10.5 days), there are now four clusters of high endothelial-cell density within the band due to the lateral motion and overlapping of the initial clusters. At the final time, $t = 10$ (15 days), in Fig. 4 we find that the endothelial-cell density distribution has now formed into a band which is slowly advancing toward the tumor, with the highest cell density at the leading edge. However, due to the form of the chosen chemotactic function (1), the cells do not reach the tumor. This models the assumed inactivation of endothelial-cell receptors for TAF (Hanahan, 1997) which causes the cells to reach a quasisteady state at approximately $x = 0.9$. However, given a long enough time, the TAF

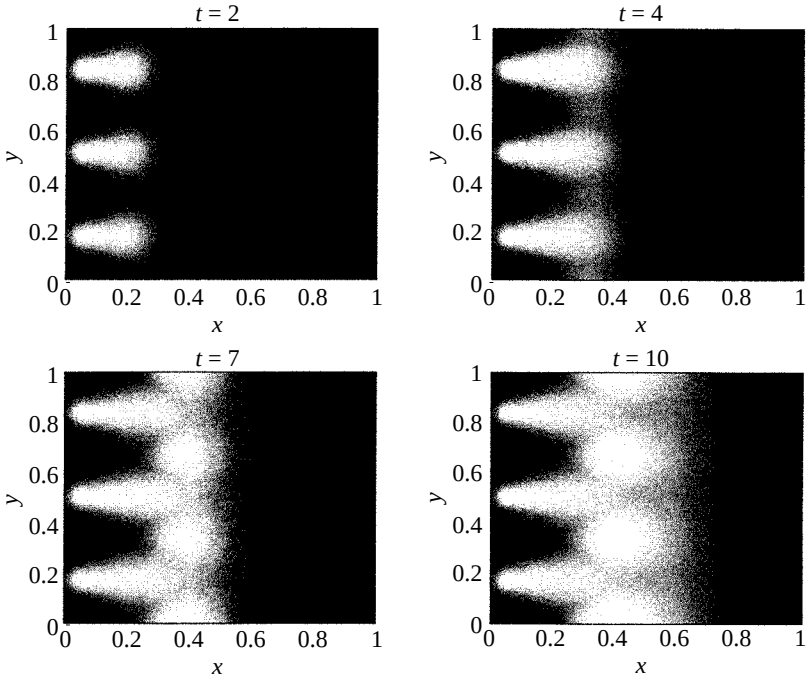

Figure 5. Plot showing the difference in fibronectin uptake between the initial fibronectin concentration and the fibronectin concentration at $t = 2$, 4, 7 and 10. The white areas represent net uptake of fibronectin by the endothelial cells. The plots show the underlying gradients of fibronectin created in the extracellular matrix, which are responsible for the behaviour of the endothelial cells in the previous figure. The color graduation is directly proportional to net fibronectin uptake, i.e., white is high uptake, black is low uptake.

concentration profile will decay to a level which will allow further cell migration. By increasing α we could restrict the extent of cell migration to a point closer to the parent vessel. This is analogous to assuming that the endothelial cells become desensitized at a lower concentration of TAF. At the other extreme, by setting $\alpha = 0$, we can ensure that the endothelial cells always reach the tumor and that vascularization occurs. The incorporation of the chemotactic function $\chi(c)$ therefore provides a potential mechanism to explain the experimental results of Sholley *et al.* (1984), which demonstrated that vascularization of the tumor did not occur in the absence of endothelial-cell proliferation.

Figure 5 shows the difference in fibronectin concentration between the initial distribution and the current distribution. The white areas represent regions where there has been a net uptake of fibronectin by the endothelial cells. This figure indicates that small gradients are being formed in the fibronectin concentration profile due to the synthesis and uptake of fibronectin by the endothelial cells. The endothelial cells then move in response to these gradients via haptotaxis.

From the results of Figs 3 and 4 it is clear that the interplay between the endothelial cells, TAF and fibronectin is capable of producing lateral movement of the cells. The incorporation of the chemotactic function $\chi(c)$ has also enabled

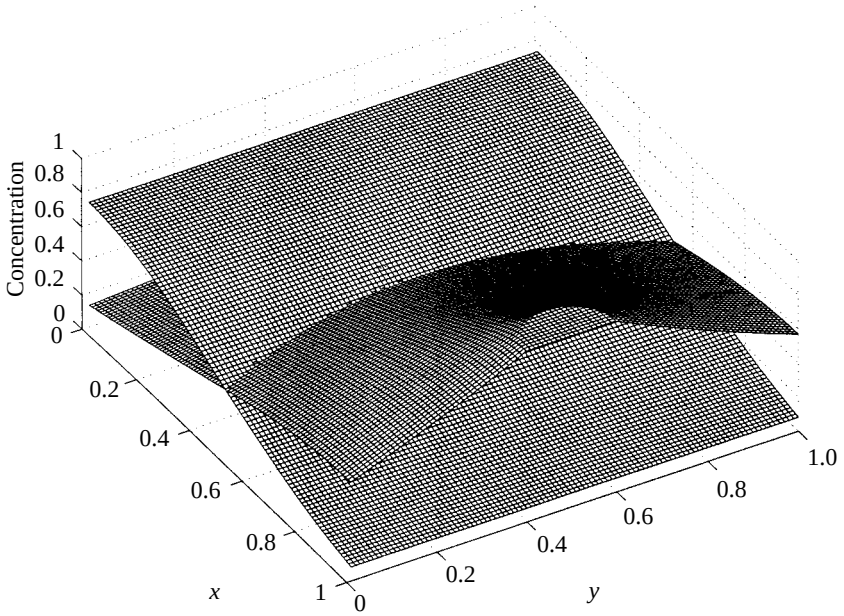

Figure 6. Initial fibronectin concentration (maximum value at $x = 0$) and initial TAF concentration profiles in the case of a circular or spherical tumor implant. The TAF concentration profile approximates a gradient produced by a circular tumor source at $x = 1, y = \frac{1}{2}$. The initial fibronectin concentration profile ($\epsilon_2 = 0.45, k = 0.75$) is unchanged from Fig. 4.

the model to reproduce the experimental observations of Sholley *et al.* (1984).

We now use our model to focus on the experimental results of Muthukkaruppan *et al.* (1982), where a single spherical tumor was implanted into the cornea of a mouse and the resulting angiogenic response was observed. This involves solving (8) numerically with an initial TAF concentration field given by (10) to represent the TAF profile generated by a circular tumor implant. Figure 6 shows the initial data for the circular TAF concentration profile (10) along with the fibronectin initial profile (13). The parameter values used were $\epsilon_2 = 0.45, k = 0.75$ and $\nu = \frac{\sqrt{5}-0.1}{\sqrt{5}-1}$. The tumor implant is centered at $(1, 0.5)$ and the value of ν was selected to ensure continuity of TAF concentration at $r = 0.1$ and a minimum concentration of TAF in the domain at $x = 0$ approximately equal to its minimum value in equation (12).

Using the above initial data and the boundary condition (9) we solved the system (8) numerically with the parameter values $D = 0.00035$, $\alpha = 0.6$, $\chi = 0.38$, $\rho = 0.34$, $\beta = 0.05$, $\gamma = 0.1$ and $\eta = 0.1$. Figure 7 shows the plots of the endothelial-cell density profiles for $t = 1$–5. The profile at time $t = 1$ (1.5 days) immediately shows the different effect of a circular tumor implant on the response of the cells, with the outer clusters of endothelial cells initially seen to be moving towards the central cluster. Comparing $t = 2$ (3 days) in Fig. 7 with Fig. 4, we see that endothelial-cell migration is somewhat slower in Fig. 7. This is due to

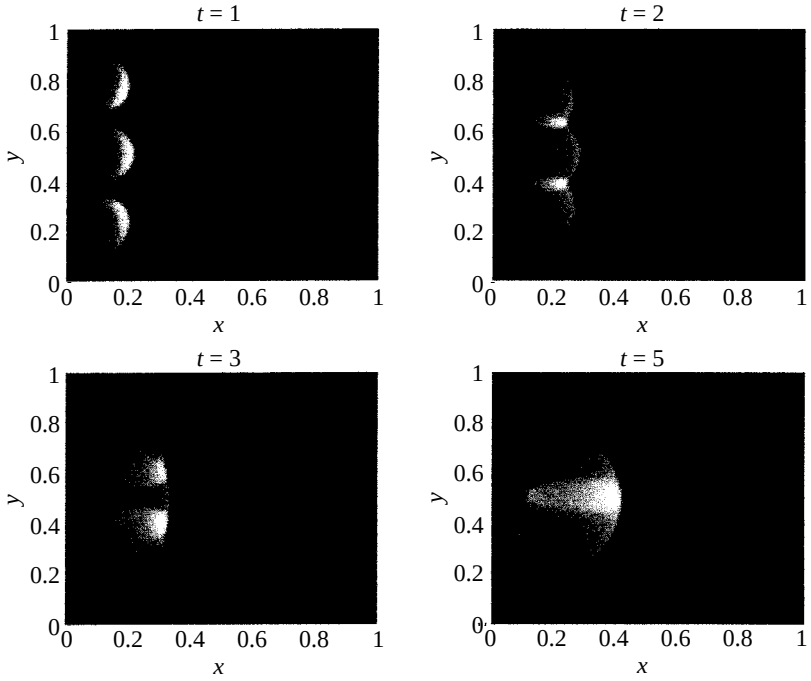

Figure 7. Spatiotemporal evolution of endothelial-cell density from a numerical simulation of system (8) representing endothelial-cell migration from the parent vessel toward a circular tumor implant with the initial fibronectin and TAF concentrations of Fig. 6 (see text for parameter values). The initial three areas of high cell density are drawn towards the centre of the domain where they coalesce and eventually form into one central area with the region of highest cell density located at the leading edge. The color graduation is directly proportional to the cell density, i.e., white is high density and black low density.

the fact that the gradient of TAF (10) is not as steep as before (12). As t increases the outer clusters move laterally and two main clusters are then formed ($t = 3$, 4.5 days). These two clusters subsequently come together to form one large central cluster of high cell density ($t = 5$, 7.5 days). Due to the slower migration of endothelial cells in Fig. 7 and the rich spatiotemporal dynamic behavior that is observed, we generated plots of the cell density distribution for later times, $t = 10$–20 (15–30 days); Fig. 8 shows the subsequent evolution of the single cluster. At $t = 10$ (15 days) we can see that there has been some lateral spread as well as both forward and backward migration of cells. There is a region of high cell density at the leading edge and also, interestingly, near the parent vessel at $x = 0$. From time $t = 12$ (18 days) to time $t = 15$ (22.5 days), regions of high cell density appear near the parent vessel and migrate forward and also laterally. By a time of $t = 20$ (30 days), a small cluster of cells has reached the tumor. At this stage interactions between the endothelial cells and the tumor cells now become important and our model is no longer valid.

The above results show how both the geometry and size of the TAF gradient is important. In changing the initial TAF concentration profile, we have been able

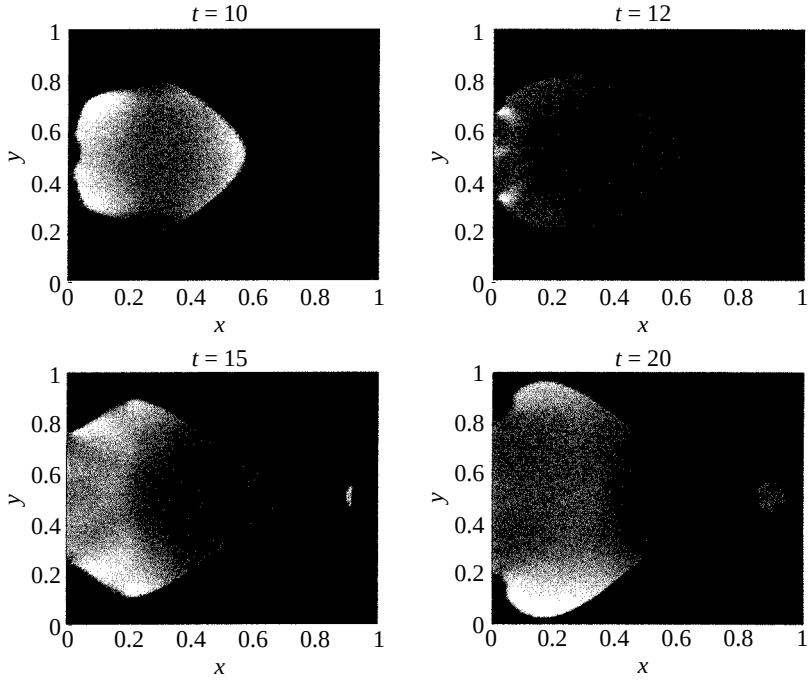

Figure 8. Spatiotemporal evolution of endothelial-cell density from a numerical simulation of system (8) representing endothelial-cell migration from the parent vessel toward a circular tumor implant for later values of t (with the same parameter values and color graduation as Fig. 7). There is now some movement of the regions of high cell density back towards the parent vessel and eventual connection with the circular tumor at some time between $t = 15$ and 20.

to produce motion of cells directed towards the tumor and also directed back towards the parent vessel. The results are due to the interplay of chemotaxis and haptotaxis and are therefore related to the distributions of both fibronectin and TAF. From the results of Figs 3–8 it is clear that our simple model (8) is capable of producing a wide range of spatiotemporal behaviour. The important points to note are as follows.

1. Without haptotaxis, the regions of endothelial-cell density migrate directly across the extracellular matrix to the tumor.
2. With haptotaxis, the regions of endothelial-cell density migrate more slowly, with lateral movement between the clusters clearly visible.
3. With an appropriate choice of α, the endothelial cells do not connect with the tumor.

We also note that the geometry of the tumor, and consequently the TAF concentration profile, clearly plays a role in influencing cell migration and therefore, the shape of the capillary network. Although these results are qualitatively realistic, since we are dealing with a continuum model, the dependent variable in the

endothelial-cell equation is endothelial-cell *density*. In the next section, we discuss a discrete form of equation (8) that enables us to follow the path of a *single* endothelial cell located at a capillary sprout tip, and hence allows us to simulate the growth of an individual capillary sprout (cf. Stokes and Lauffenburger, 1991).

4. THE DISCRETE MATHEMATICAL MODEL

Many different types of discrete models, such as coupled map lattice models, fractal models, diffusion limited aggregation models and L-systems, have already been developed to model general branching processes (including angiogenesis) in a qualitative and phenomenological way (Bell *et al.*, 1979; Bell, 1986; Gottlieb, 1990, 1991a, b; Düchting, 1990a, 1990b, 1992; Prusinkiewicz and Lindenmayer, 1990; Kiani and Hudetz, 1991; Landini and Misson, 1993; Indermitte *et al.* 1994; Düchting *et al.*, 1996; Nekka *et al.*, 1996). These discrete models may be considered as particular examples of a wider class of discrete models, referred to generically as cellular automata models, which have been applied to a wide range of problems in many areas of applied mathematics. An excellent survey of cellular automata models applied specifically to biological systems can be found in the paper of Ermentrout and Edelstein-Keshet (1993). Cellular automata models are discrete in time, space and state. They have the advantage of being computationally fast and efficient, and can provide qualitative information regarding a particular model without necessarily having to provide exact parameter values. They are also useful for providing a foundation upon which one can construct a more detailed and precise mathematical model. However, one of the main problems with cellular automata models is in defining the appropriate state space. In certain situations, the transition from one state to another is clear, but, in general, such distinctions do not exist. The spatial movement of individuals in cellular automata models is governed mainly by nearest-neighbor interactions and as such shares some similarity with the discrete model we will present below. However, in general, the nearest-neighbor interactions for cellular automata models are based on phenomenological rules, whereas, in our discrete model, the movement rules are based directly on a discretized form of the continuous model (8).

In this section we will develop a novel discrete mathematical model of tumor-induced angiogenesis which will enable not only a qualitative but also a quantitative comparison with *in vivo* experimental results. The model will be based around the assumption that the motion of an individual endothelial cell located at the tip of a capillary sprout governs the motion of the whole sprout. This is not unreasonable since the remaining endothelial cells lining the sprout-wall are contiguous (Paweletz and Knierim, 1989; Stokes and Lauffenburger, 1991). The particular technique which we will use to follow the path of an individual endothelial cell at a sprout tip is a development of the method used by

Anderson *et al.* (1997) and first of all involves discretizing (using standard finite-difference methods) the partial differential equation governing the rate of change of endothelial-cell density (8). We then use the resulting coefficients of the five-point finite-difference stencil to generate the probabilities of movement of an individual cell in response to its local milieu. This technique differs from the discrete model of Stokes and Lauffenburger (1991) in that the movement of individual cells is based on a discrete form of the continuous model, but is similar to that used by Weimar *et al.* (1992a, b) (wave propagation in excitable media) and that of Dallon and Othmer (1997) (aggregation of *Dictyostelium discoideum*). However, there is an element of stochasticity (randomness) in our model in the movement rules for the cells. In effect, we will derive a biased random-walk governing the motion of a single endothelial cell based on the system of partial differential equations (8). In this sense, our discrete model is probably most similar in formulation to the reinforced random-walk models of Othmer and Stevens (1997), where cell movement is modeled in response to a chemical stimulus by considering an equation (discrete in space and continuous in time) governing the probability that a cell is at a given position at time t. This equation is a function of the transition probabilities for one-step jumps to the orthogonal neighbors. The form of the transition probabilities for the gradient model of Othmer and Stevens (1997) is very similar to the probabilities of movement that will be derived from our discrete model (see also Alt, 1980; Davis, 1990).

We now set about formulating the discrete model and deriving the movement probabilities for an individual endothelial cell located at a sprout tip. Rules for processes such as the generation of new capillary sprouts (branching) and the fusion of two sprouts (anastomosis) will be described later. We first discretize (8) using the Euler finite difference approximation (Mitchell and Griffiths, 1980). This involves approximating the continuous two-dimensional domain $[0, 1] \times [0, 1]$ in the usual way as a grid of discrete points (mesh size h), and time (t) by discrete increments (magnitude k). The full discretized system is given in the Appendix. For clarity we only consider the endothelial-cell equation,

$$n_{l,m}^{q+1} = n_{l,m}^{q} P_0 + n_{l+1,m}^{q} P_1 + n_{l-1,m}^{q} P_2 + n_{l,m+1}^{q} P_3 + n_{l,m-1}^{q} P_4, \qquad (14)$$

where the subscripts specify the location on the grid and the superscripts the time steps. That is $x = lh$, $y = mh$ and $t = qk$ where l, m, k, q and h are positive parameters.

In a numerical simulation of the continuous model (8), the purpose of the discrete equation (14) is to determine the endothelial-cell density at grid position (l, m), and time $q + 1$, by averaging the density of the four surrounding neighbors at the previous time step q. For our discrete model, we will use the five coefficients P_0–P_4 from equation (14) to generate the motion of an individual endothelial-cell. These coefficients can be thought of as being proportional to

the probabilities of the endothelial cell being stationary (P_0) or moving left (P_1), right (P_2), up (P_3) or down (P_4).

Each of the coefficients P_1–P_4 consists of three components,

$$P_n = \text{random movement} + \text{chemotactic} + \text{haptotactic}, \tag{15}$$

thus showing how the discrete endothelial-cell equation is linked to the continuous endothelial-cell equation of system (8). The coefficient P_0 has a similar form (see Appendix). Equation (15) is very similar to the transition probabilities of the reinforced random-walk model of Othmer and Stevens (1997). In particular, their gradient models have a random component and a 'taxis' component. Othmer and Stevens (1997) used their discrete transition probabilities to then derive a partial differential equation in the continuous limit. It is possible to show this for our model by defining transition probabilities of the form (15). The original equation governing the rate of change of endothelial-cell density (8) can then be recovered by following the analysis of Othmer and Stevens (1997) in the same rigorous manner.

The exact forms of P_0–P_4 involve functions of the fibronectin and TAF concentrations near an individual endothelial cell (see Appendix). Therefore, if there were no fibronectin or TAF the values of P_1–P_4 would be equal, with P_0 smaller (or larger, depending on the precise values chosen for the space and time steps), i.e., there is no bias in any one direction and the endothelial cell is less (more) likely to be stationary—approximating an unbiased random-walk. However, if there is a TAF gradient and no fibronectin gradient, chemotaxis dominates and the coefficients P_0–P_4 will become biased towards the tumor source at $x = 1$ (see Fig. 3 for continuous results). The reverse is true if there is only a fibronectin gradient and no TAF gradient, i.e., haptotaxis dominates. When both gradients exist, the complex interplay between chemotaxis and haptotaxis will bias the coefficients accordingly. The motion of an individual cell at the sprout tip is therefore governed by its interactions with angiogenic factors and matrix macromolecules in its local environment.

Before proceeding to the simulation section, we first of all discuss the manner in which we explicitly incorporate the processes of branching and anastomosis into the discrete model.

4.1. ***Rules for branching and anastomosis.*** While there is a good deal of information regarding the actual events of the generation of new sprouts (sprout branching) and the formation of loops (anastomosis), there is no explanation as to the precise mechanisms which cause them (Paweletz and Knierim, 1989). Figure 9 gives a schematic illustration of these processes which we will model explicitly using the discrete model.

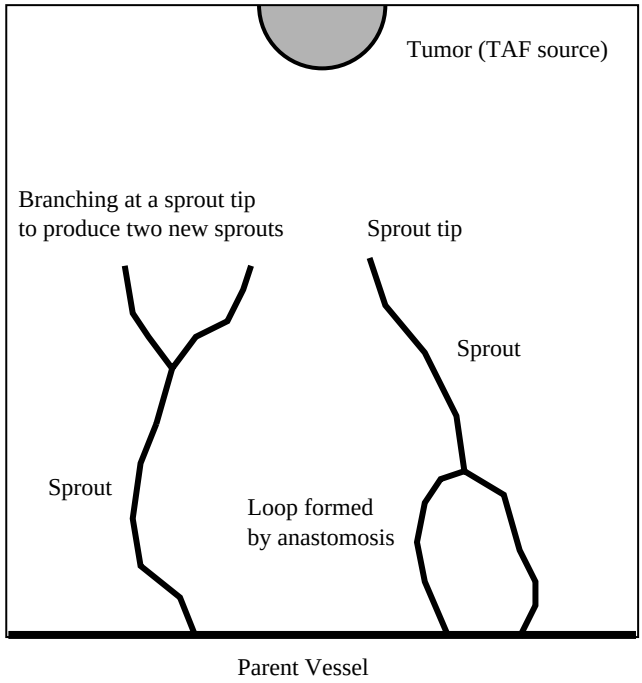

Figure 9. Schematic representation of branching at a capillary sprout tip to produce two new sprouts and anastomosis of two capillary sprouts to form a loop.

We will assume that the generation of new sprouts (branching) occurs only from existing sprout tips. It is also reasonable to assume that the newly formed sprouts are unlikely to branch immediately and that there must be a sufficient number of endothelial cells, near the sprout tip, for new sprouts to form. We will assume that the density of endothelial cells required for branching is inversely proportional to the concentration of TAF, since the new sprouts become much shorter as the tumor is approached, i.e., as the TAF concentration increases (cf. Muthukkaruppan *et al.*, 1982). From these assumptions we obtain the following three conditions, which must be satisfied before a capillary sprout can branch at its tip and generate a new sprout.

1. The age of the current sprout is greater than some threshold branching age ψ, i.e., new sprouts must mature for a length of time at least equal to ψ before being able to branch.
2. There is sufficient space locally for a new sprout to form, i.e., branching into a space occupied by another sprout is not possible.
3. The endothelial-cell density is greater than a threshold level n_b, where $n_b \propto \frac{1}{c_{l,m}}$.

We note that these conditions have been chosen as one possible method for producing new sprouts (branching) and that other equally valid choices are possible.

Given that each of the above three conditions is satisfied, we assume that each sprout tip has a probability, P_b, of generating a new sprout (branching) and that

this probability is dependent on the local TAF concentration. We therefore adopt a positional information approach (Lewis *et al.*, 1977; Wolpert, 1981), with the simple rule that, as the TAF concentration increases, the probability of generating new sprouts (branching) increases. Figure 10 shows how the probability of generating new sprouts (branching) varies with TAF concentration and subsequently with space. The branching probabilities have been chosen on a qualitative basis, i.e., very little branching occurs initially (near the parent vessel, e.g., limbus), but as the endothelial cells migrate closer to the tumor (at $x = 1$) the number of new sprouts slowly increases. A short distance from the tumor the frequency of branching dramatically increases creating the 'brush border' effect.

Anastomosis, the formation of loops by capillary sprouts, is another very important feature of angiogenesis which can be captured explicitly by the discrete model. As the sprouts progress towards the tumor, driven by the movement probabilities of (14), at each time step of the simulation, the endothelial cells at the sprout tips can move to any of the four orthogonal neighbors on the discrete grid. If upon one of these moves another sprout is encountered, then anastomosis can occur. Experiments have shown that the initial formation of anastomoses occurs at a well-defined distance from the parent vessel (Paweletz and Knierim, 1989). For simplicity, we assume that, as a result of the anastomosis, only one of the original sprouts continues to grow (the choice of which is purely random). The schematic diagram of Fig. 9 shows the formation of a loop by anastomosis of two individual capillary sprouts.

4.2. ***Simulation process for the discrete model.*** Each time step of the simulation process involves solving the discrete form of the system (8) numerically to generate the five coefficients P_0–P_4 (see Appendix). Probability ranges are then computed by summing the coefficients to produce five ranges, $R_0 = 0$–P_0 and $R_j = \sum_{i=0}^{j-1} P_i$–$\sum_{i=0}^{j} P_i$, where $j = 1$–4. We then generate a random number between 0 and 1, and, depending on the range into which this number falls, the current individual endothelial cell under consideration will remain stationary (R_0) or move left (R_1), right (R_2), up (R_3) or down (R_4). The larger a particular range, the greater the probability that the corresponding coefficient will be selected. Each endothelial cell is therefore restricted to move to one of its four orthogonal neighboring grid points or remain stationary at each time step.

All the simulations of the discrete model were carried out on a 200×200 grid, which is a discretization of the unit square, $[0, 1] \times [0, 1]$, with a space step of $h = 0.005$. Given that our unit of length is 2 mm, this means that h is equivalent to a dimensional length of 10 μm, i.e., approximately the length of one or two endothelial cells (Paku and Paweletz, 1991). A discrete form of the no-flux boundary condition (9) was imposed on the square grid, restricting the endothelial cells to within the grid. The initial conditions in all simulations (unless otherwise stated) are given by discrete forms of the fibronectin (13) and TAF (12) equations. We assume that there are five capillary sprouts initiated by

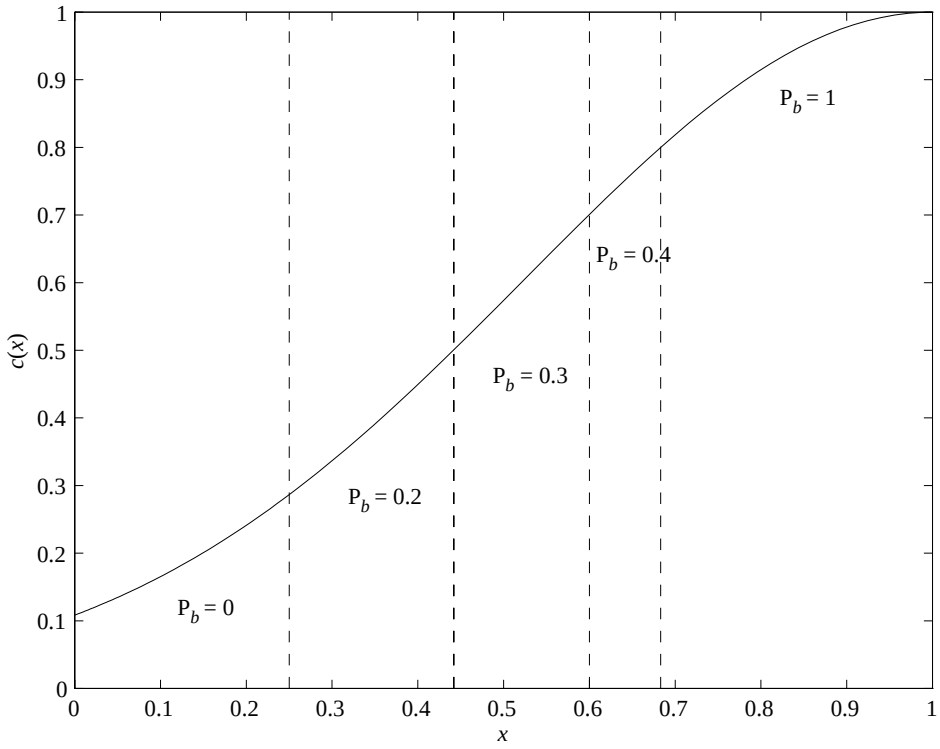

Figure 10. Positional branching probabilities in relation to the TAF concentration. The probability of branching increases as the TAF concentration increases, i.e., as the tumor, located at $x = 1$, is approached.

five endothelial cells located at the sprout tips. Three of them are located at the maximum-density positions of the continuous endothelial-cell initial data (Fig. 2) and the other two being placed between these. Therefore, we have endothelial cells starting at $y = 0.17,\ 0.3,\ 0.5,\ 0.65,\ 0.84$ all at $x = 0$.

The parameter values used in the following simulations are the same as those used in the previous two-dimensional continuous simulations (unless otherwise stated), i.e., $D = 0.00035$, $\alpha = 0.6$, $\chi = 0.38$, $\rho = 0.34$, $\beta = 0.05$, $\gamma = 0.1$ and $\eta = 0.1$. Through trial and error it was found that a threshold branching age of $\psi = 0.5$ (equivalent to a dimensional time of 0.75 days) produced simulated networks which were qualitatively similar in morphology to those networks observed *in vivo*.

4.3. ***Discrete model simulation results.*** As with the continuous two-dimensional simulations we will initially consider our discrete model without the effect of haptotaxis, i.e., $\rho = 0$. Figure 11 shows four snapshots in time of the capillary sprouts progressing towards the tumor. The progress of the sprouts is almost linear in each case, with little lateral motion (i.e., parallel to the y-axis) and no contact between the initial sprouts and, therefore, no anastomosis. As the sprouts

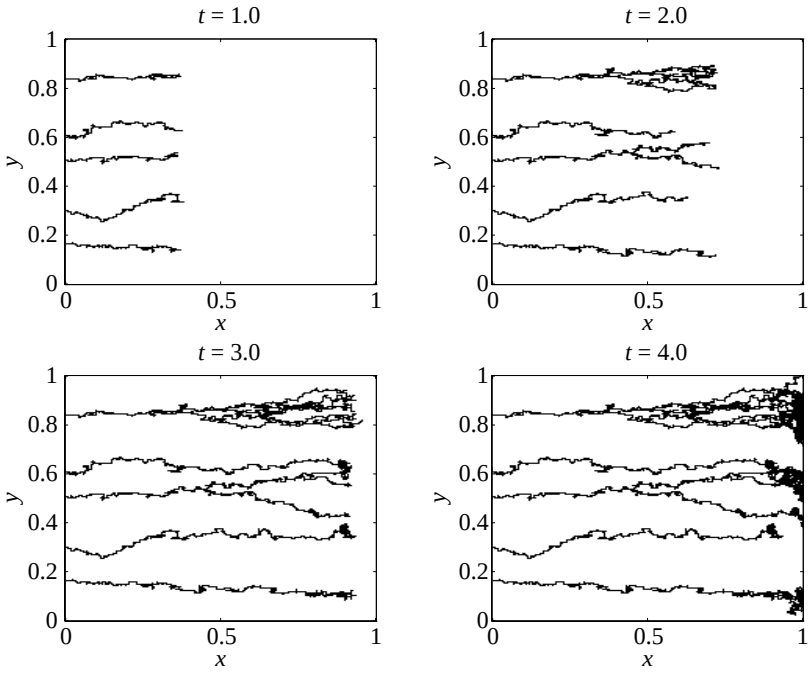

Figure 11. Spatiotemporal evolution of a capillary network from a numerical simulation of the discrete model. The figure shows the endothelial cells at the capillary sprout tips migrating from the parent vessel ($x = 0$) towards a line source of tumor cells ($x = 1$) in the absence of haptotaxis (see text for parameter values). We observe that there is very little lateral movement (in the y direction) or branching, no anastomosis and by $t = 4$ the sprouts connect with the tumor.

progress and near the tumor, there is a minimal amount of branching. Comparing these results with the continuous equivalent in Fig. 3, we see that the sprout progression matches well with the movement of the high areas of endothelial-cell density. Owing to the inherent randomness of the discrete model, some of the sprouts progress more slowly than others in Fig. 11. To show how the geometry of the TAF concentration profile affects both the full system and the chemotaxis-only system we use the same parameter values as above (i.e., no haptotaxis) but with a discrete form of the circular TAF initial data (10). The four plots in Fig. 12 show clearly how all five initial sprouts are drawn together towards the maximum TAF concentration at $(1, \frac{1}{2})$. There is some branching, but again there is no anastomosis. Although some of the sprouts do encounter each other, they do so far into the domain.

We next consider the model with the inclusion of haptotaxis. Using the original initial data [i.e., linear profiles of TAF/fibronectin gradients from equations (12) and (13)] with the haptotaxis coefficient $\rho = 0.34$ and the other parameters as before, we generated the plots shown in Fig. 13. At $t = 3$ we see that anastomosis has occurred between the second and third sprouts (from the top), and also that the migration of the endothelial cells is slower than the chemotaxis-only results

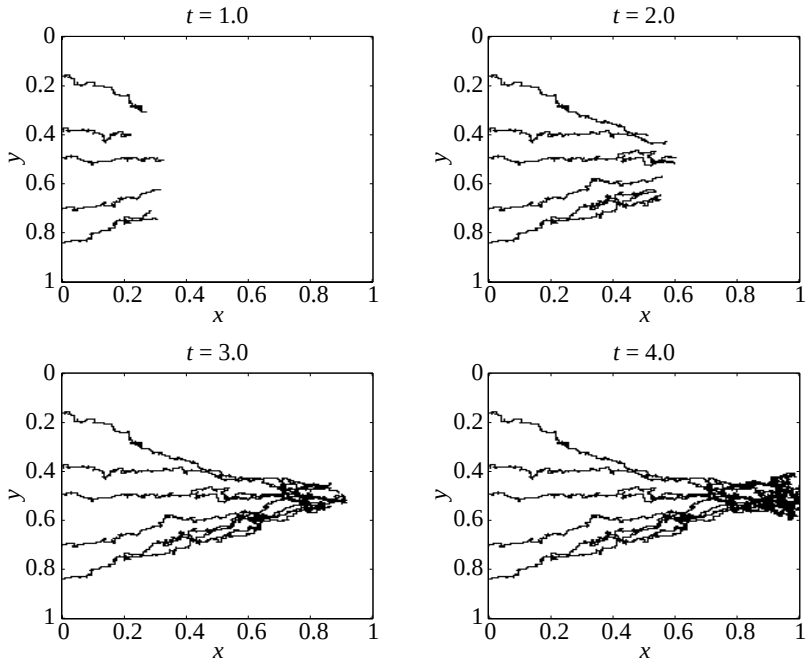

Figure 12. Spatiotemporal evolution of a capillary network from a numerical simulation of the discrete model. The figure shows the migration of endothelial cells at the capillary sprout tips in the absence of haptotaxis towards a circular TAF source, with the same parameter values as Fig. 11. In this case the sprouts converge towards the middle of the domain, but this is due solely to the circular geometry of the TAF concentration profile. Very little anastomosis occurs and again the sprouts connect with the tumor by $t = 4$.

of Fig. 11. The lateral movement of sprouts in this case is governed solely by haptotaxis and the interactions of the endothelial cells with the extracellular matrix and not the geometry of the TAF concentration profile. As t increases, the sprouts begin to branch and spread into the domain, contrasting with the linear, compact endothelial-cell migration of the chemotaxis-only results (Fig. 11). As the tumor is approached, the sprouts coalesce and form the 'brush border' observed by Muthukkaruppan *et al.* (1982). Comparing the time $t = 7.5$ with $t = 7$ in the continuous results (Fig. 4) we again see that the two match well.

We now discuss the simulations of endothelial-cell movement towards a circular TAF source (representing a small solid tumor implant) and use a discrete form of (10) with the parameter values the same as in Fig. 13. By $t = 3$ in Fig. 14, we see that two of the sprouts have already achieved anastomosis, with another two about to form a loop, and that one of the sprouts near $y = 0.3$ appears to be moving away from the tumor back towards the parent vessel. This same sprout continues to move towards the parent vessel ($x = 0$) until it reaches a steady state between $t = 15$ and 20. Cell migration towards the tumor is slower than in Fig. 13 which agrees well with the continuous results of Figs 7 and 8. This is due, in part, to the shallower gradient of the circular TAF concentration initial

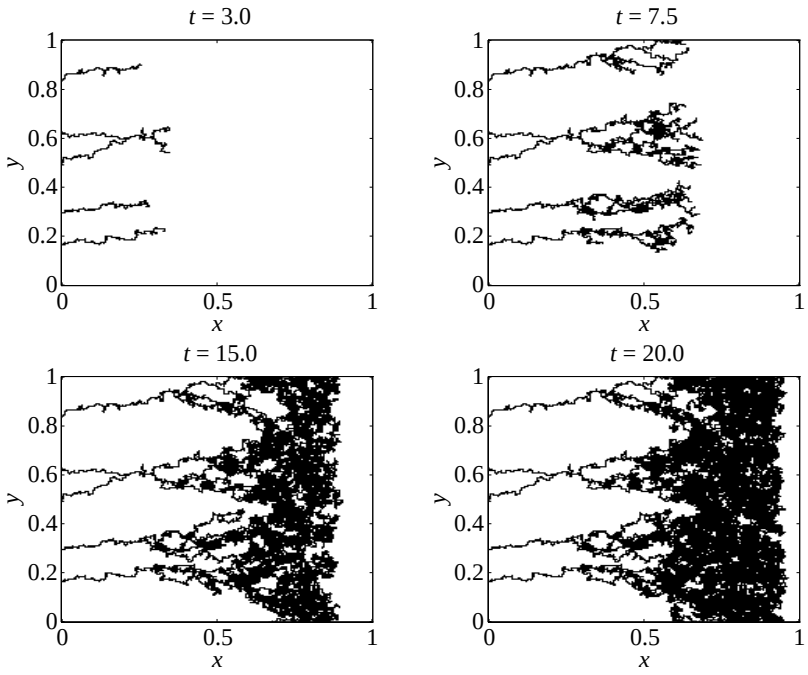

Figure 13. Spatiotemporal evolution of a capillary network from a numerical simulation of the discrete model. The figure shows the migration of endothelial cells at the capillary sprout tips under the influence of both chemotaxis and haptotaxis towards a line source of tumor cells situated at $x = 1$, with the same parameter values as Fig. 4. Anastomosis of the second and third sprouts (from the top) and the branching of all sprouts is observed. The formation of the dense 'brush border' is also evident.

data. The 'brush border' occurs further from the tumor than in Fig. 13, again due to the gradient difference and subsequently the stronger haptotactic effect of fibronectin. Comparing the profiles at $t = 15$ and 20 in Fig. 8 with those in Fig. 14, the high-density regions are in good agreement with the results of the discrete model. The simulations of Fig. 12 in comparison with those of Fig. 14 emphasize the importance of cell–matrix interactions via haptotaxis in achieving both anastomosis and the generation of a sufficient vasculature.

The absence of cell proliferation in the model prevents the completion of angiogenesis and this is seen in both the continuous and discrete results (Figs 3 and 12). This is due to the incorporation of the chemotactic function $\chi(c)$, enabling us to reproduce the experimental observations of Sholley *et al.* (1984) which demonstrated that vascularization of the tumor did not occur in the absence of cell proliferation. Due to the choice of parameters the sprouts reach a steady state at $x \approx 0.9$. By increasing the parameter α we are able to restrict the extent of the network to a point closer to the parent vessel. This is analogous to assuming that the endothelial cells become desensitized at a lower concentration of TAF. In order to accomplish vascularization, the endothelial cells must proliferate and subsequently migrate the whole distance to the tumor. The incorporation of

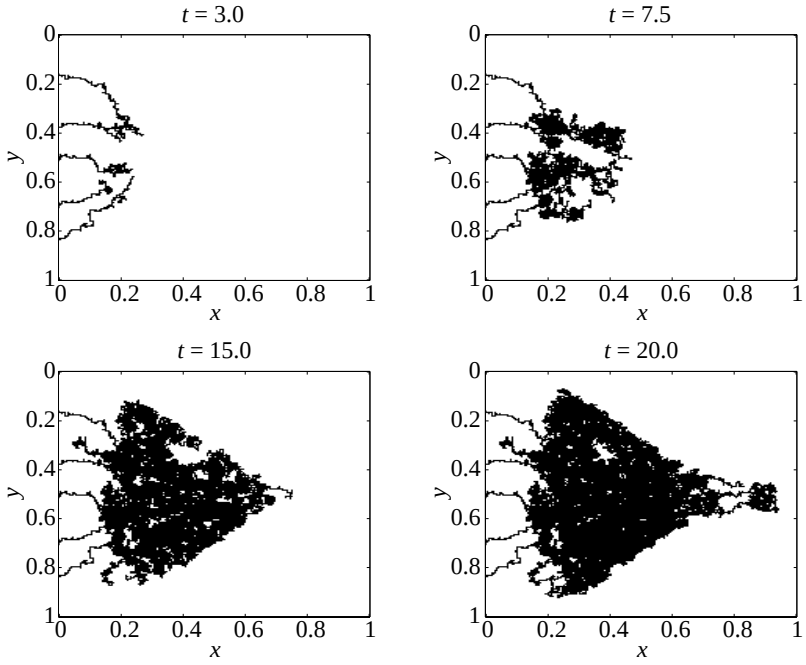

Figure 14. Spatiotemporal evolution of a capillary network from a numerical simulation of the discrete model. The figure shows the migration of endothelial cells at the capillary sprout tips under the influence of both chemotaxis and haptotaxis towards a circular tumor implant, with the same parameter values as Fig. 7. Four of the five initial sprouts achieve anastomosis and some sprouts are also seen to migrate backwards, i.e., away from the tumor toward the parent vessel. Once again the formation of the 'brush border' is clearly observed.

proliferation in the discrete model will be considered in the next section.

Finally, Fig. 15 shows the results of a simulation with a constant initial distribution of fibronectin as an initial condition, i.e., $f(x, y, 0) = 0.4, \forall x, y \in [0, 1] \times [0, 1]$. This represents a homogeneous initial distribution of pre-existing fibronectin in the extracellular matrix. The initial TAF concentration profile was taken to be the discrete form of (12). From the results shown in this figure, it is clear that the structure of the capillary network produced is qualitatively similar to the network structure of Fig. 13, but, due to the absence of an initial fibronectin gradient, the network progresses towards the tumor more quickly. These results indicate that the precise initial distribution of fibronectin is not of crucial importance in generating a realistic branched network. However, as we have shown from the results of Fig. 11, the presence of fibronectin, or more precisely, interaction between the cells and the extracellular matrix, is required for the generation of realistic network structures.

4.4. ***Cell proliferation.*** As discussed in the introduction, during angiogenesis there is initially no endothelial-cell proliferation. Cells are recruited from the

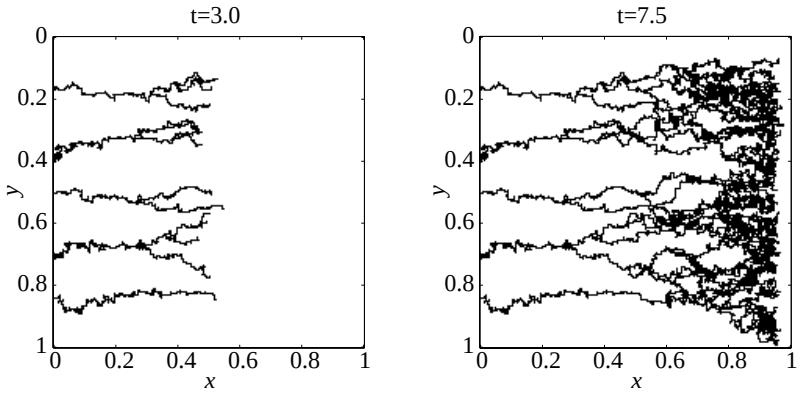

Figure 15. Spatiotemporal evolution of a capillary network from a numerical simulation of the discrete model. The two plots show the migration of endothelial cells at the capillary sprout tips under the influence of both chemotaxis and haptotaxis with a constant, homogeneous distribution of fibronectin [$f(x, y, 0) = 0.4$] and a linear source of tumor cells as initial conditions. The two plots clearly show the development of a branched network which is similar in structure to that of Fig. 13.

parent vessel and migrate toward the tumor. Approximately 36–48 h into the process, cell mitosis is observed (Sholley *et al.*, 1984; Paweletz and Knierim, 1989) and is confined to a region just behind the sprout tip. Endothelial-cell doubling time has been estimated at 18 h (Williams, 1987) and we model the process of cell division in the discrete model by assuming that some of the cells behind the sprout tip divide (into two daughter cells) every 18 h. We assume that this has the effect of increasing the length of a sprout by approximately one cell length every 18 h. In terms of the non-dimensional discrete model, this is equivalent to the sprout length being increased by an amount h every half time unit. Owing to the inherent randomness of the discrete model, proliferation will occur asynchronously in separate sprouts, as is observed experimentally (Paweletz and Knierim, 1989). This feature is captured by the discrete model as the age of each cell at a sprout tip is known and this determines when mitosis occurs. Figure 16 gives a schematic illustration of this process.

Figure 17 shows the results of incorporating endothelial-cell proliferation in the discrete model as described above, with a linear source of tumor cells located at $x = 1$. The parameter values and initial conditions for fibronectin and TAF are as shown in Fig. 13. Cell proliferation is assumed to begin 48 h into the process, i.e., at a (non-dimensional) time of $t = 1.3$, and cell doubling is assumed to occur every 18 hr ($t = 0.5$). By $t = 3$ sprouts two and three (from the top) have almost formed a loop. At this stage there is little difference between this developing network and the corresponding network in Fig. 13. However, by $t = 7.5$, we see that a well-developed branching network has already formed, with proliferation providing additional extension of the sprouts, and by $t = 10$, the sprouts have already connected with the tumor. This is in contrast with the corresponding network in Fig. 13.

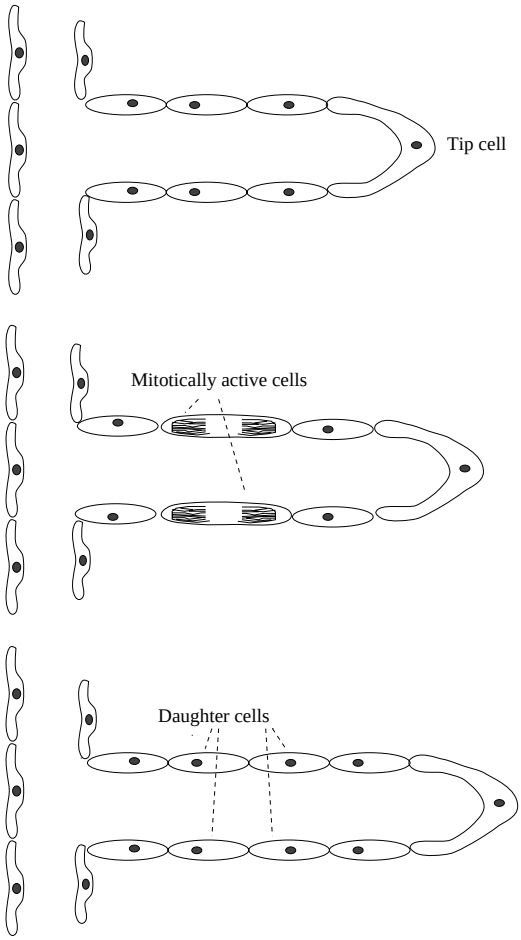

Figure 16. Schematic representation of cell proliferation and subsequent sprout extension. Cells behind the sprout tip undergo mitosis. Each of these mitotic cells divides and gives rise to two daughter cells. The effect of this process is to extend the overall length of the capillary sprout.

Figure 18 shows the results of incorporating endothelial-cell proliferation in the discrete model (as described above), but this time with a circular tumor implant. The parameter values and initial conditions for fibronectin and TAF are as per Fig. 14. From the plots at $t = 3$ and $t = 7.5$, one can see that the developing network is very similar in structure to that in Fig. 14. However, once again, by $t = 10$ the sprouts have already connected with the tumor (in contrast with Fig. 14) with the final structure of the network in Fig. 18 being less dense than that in Fig. 14.

5. DISCUSSION AND CONCLUSIONS

The work we have presented here has developed a mathematical model for tumor-induced angiogenesis using a novel blend of continuum, deterministic

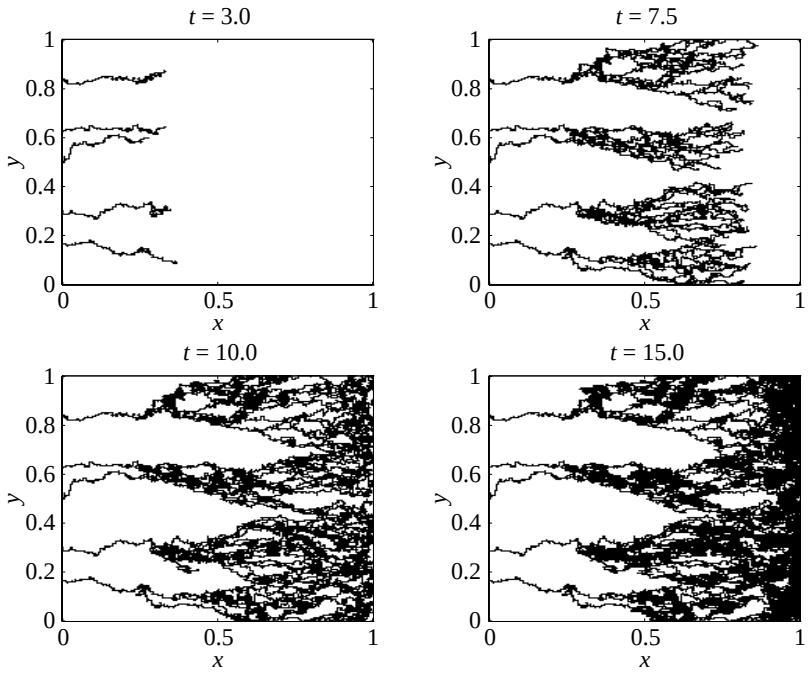

Figure 17. Spatiotemporal evolution of a capillary network from a numerical simulation of the discrete model. The figure shows the migration of endothelial cells at the sprout tips (with both chemotaxis and haptotaxis) towards a line source of tumor cells with endothelial-cell proliferation. The network connects with the tumor after a time of $t = 10$ and vascularization is achieved.

modeling and discrete, stochastic modeling in two space dimensions. Parameter values for the models (in particular the length scale L, the cell random-motility coefficient D_n, the TAF diffusion constant D_c, the chemotactic coefficient χ_0 and the endothelial-cell proliferation rate) were estimated, as far as possible, from independent experimental measurements, thus grounding the results of the model in a realistic framework.

The continuum model consists of a system of nonlinear partial differential equations and examines how endothelial cells respond not only to angiogenic cytokines (such as VEGF) via chemotaxis, but also to essential interactions with extracellular matrix macromolecules (such as fibronectin) via haptotaxis. The results from the continuum-model simulations demonstrate two important aspects of capillary-network formation. First, in agreement with previous models (e.g., Stokes and Lauffenburger, 1991; Chaplain and Stuart, 1993), a sufficiently strong chemotactic response is necessary for the initial outgrowth of the capillary network. Secondly, the model demonstrates the importance of interactions between endothelial cells and the extracellular matrix. The inclusion of uptake terms for the TAF and fibronectin by the cells enables the creation of local gradients around the areas of high cell density which permits lateral migration. Without such interactions, the model predicts that the cells move directly to the tumor without any

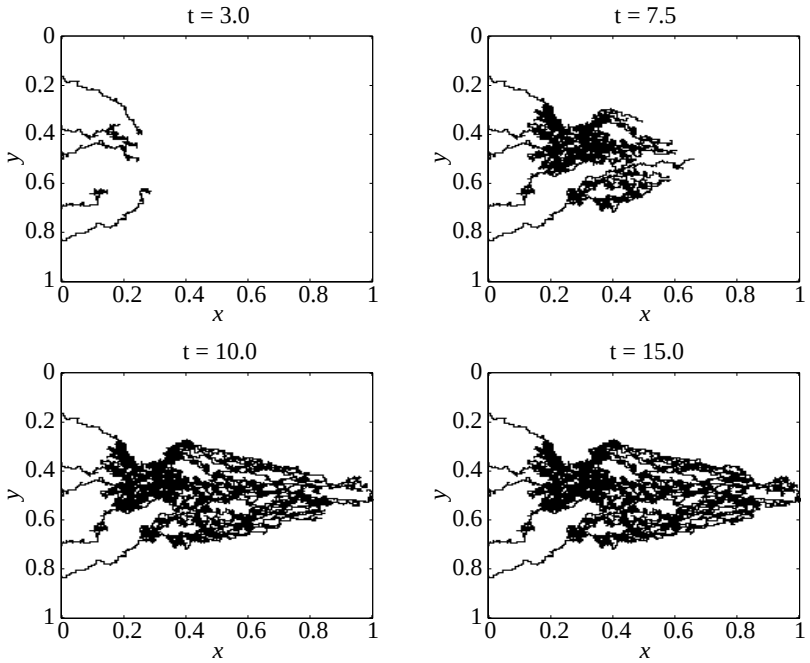

Figure 18. Spatiotemporal evolution of a capillary network from a numerical simulation of the discrete model. The figure shows the migration of endothelial cells at the sprout tips (with both chemotaxis and haptotaxis) towards a circular source of tumor cells with endothelial-cell proliferation. Once again the network connects with the tumor around $t = 10$ and vascularization is achieved.

significant lateral movement. These results show that the important large-scale features of angiogenesis can be captured qualitatively using a continuum model. However, important processes on a smaller scale, such as sprout branching, are not captured. This requires the development of a discrete model applicable at the level of a single endothelial cell.

The discrete model that we developed was derived from a discretized form of the partial differential equations of the continuum model, and permits the tracking of individual endothelial cells located at the capillary sprout tip. This, in turn, enables the path of the complete capillary sprout to be followed. Since the parameter values used in the discrete model are directly related to those of the continuum model, the results of the simulations of the discrete model are therefore also firmly grounded in a realistic framework. In addition to this, the discrete model enables us to explicitly incorporate rules for the production of new sprouts (branching), the fusion of sprouts to form loops (anastomosis) and sprout extension through endothelial-cell proliferation. The results from the discrete model simulations confirm the predictions of the continuum model that both chemotaxis and haptotaxis are necessary for the formation of a capillary network at a large scale.

On a finer scale, the discrete model simulations produce capillary networks

with a very realistic structure and morphology, capturing the early formation of loops (anastomosis), the essential dendritic structure of a capillary network and the formation of the experimentally observed 'brush border'. The discrete model also incorporates a realistic method of modeling mitosis and its effect on the sprouts, i.e., actual extension in the length of the sprout due to cell division.

Owing to the manner in which the discrete model is derived [finite difference approximation of equation (8)] and subsequently developed (the inclusion of branching, anastomosis and sprout extension via cell proliferation) and then simulated [using the coefficients of equation (14) as probabilities of cell movement], it shares some similarities with previous discrete models (Weimer *et al*., 1992a, b), previous stochastic differential equation models (Stokes and Lauffenburger, 1991) and, most closely, with reinforced (or biased) random-walk models (Othmer and Stevens, 1997). While reinforced random-walk models have not as yet been applied to modeling angiogenesis, the probabilities governing endothelial-cell movement in our discrete model are very similar to the transition probabilities for cell movement in the gradient models of Othmer and Stevens (1997) where such transition probabilities are taken as the basis for deriving a continuum approximation. If we apply this same procedure to the movement probabilities of equation (15), we obtain a more general equation describing cell movement, with arbitrary functional forms for $\chi(c)$ and $\rho(f)$. The equation for endothelial-cell density in equation (8) can then be recovered by taking $\chi(c)$ to have the form of equation (1) and choosing $\rho(f) = \rho$. This procedure demonstrates, in a rigorous manner, the link between the individual cell level and the population level.

Our discrete modeling techniques are therefore different to the discrete model of angiogenesis of Stokes and Lauffenburger (1991), which is the closest comparable model of angiogenesis at the individual cell level. Moreover, the inclusion of fibronectin production and uptake by the endothelial cells, cell–matrix interactions via haptotaxis, TAF uptake by the endothelial cells, and a more realistic approach to the effects of cell proliferation on the extension of the sprouts, significantly extends the work of Stokes and Lauffenburger (1991).

The results of the discrete model simulations emphasize the importance of cell–matrix interactions in producing lateral motion of the sprouts. Subsequent loop formation is, therefore, also dependent upon cell–matrix interactions. By increasing the cell random motility coefficient by a factor of 10, therefore bringing this parameter value in line with that used by Stokes and Lauffenburger (1991), we generated capillary networks which were rather more disorganized and lacking in structure. Experimental observations (Paweletz and Knierim, 1989; Paku and Paweletz, 1991) indicate that there this is very little random motility of endothelial cells at the sprout tips, which is in line with the assumptions and results of our model. These findings are in contrast with the results of Stokes and Lauffenburger (1991) where cell random motility played a crucial role in determining the anastomosis of sprouts—without a sufficiently strong cell random motility response, there was little loop formation. Finally, in the discrete

model simulations, the timescale on which the capillary network formed (between 10 and 21 days in real time) correlates very well with experimental observations (Gimbrone *et al.*, 1974; Ausprunk and Folkman, 1977; Muthukkaruppan *et al.*, 1982).

We have also carried out simulations with an increased value for the chemotactic coefficient χ, keeping ρ fixed. This leads to the capillary network reaching the tumor in a shorter time and having a structure similar to those of the chemotaxis-only results in Fig. 11, i.e., there was not as much lateral movement of the sprouts and not as much branching of the sprouts. Other simulations using alternative initial distributions of fibronectin (e.g., constant concentration throughout the domain, cf. Fig. 15; less steep initial gradients) lead to capillary network structures having very similar overall morphology to the results presented in Figs 13 and 14. However, the presence of fibronectin in the matrix and a haptotactic response from the endothelial cells is essential for realistic structures to be generated. These results would seem to imply an optimal chemotactic–haptotactic response for the formation of a sufficiently well-connected vasculature. Finally, simulations involving a range of different values of the parameters β, γ and η between 0 and 1, indicated that the system is not particularly sensitive to changes in these parameters.

Although the model has incorporated many of the important mechanisms involved in the angiogenic process, some extensions of the model are still possible. There is now clear experimental evidence that disrupting the transmembrane receptor tyrosine kinases (RTKs) has a direct effect on the structural morphogenesis of the capillary network. Results show that disrupting the RTK Tie2 receptor of endothelial cells leads to a poorly formed capillary network which lacks a full branching structure (Dumont *et al.*, 1994; Sato *et al.*, 1995; Hanahan, 1997). Therefore, the number of active receptors on the cell surface can have a direct influence on the outcome of network structure. One way to extend the model further would therefore be to consider the chemotactic function $\chi(c)$ as an explicit function of the number of active TAF receptors, i.e., we could include an extra equation for the receptor kinetics and couple this directly into the chemotactic function (cf. Sherratt *et al.*, 1993; Sherratt, 1994; Höfer *et al.*, 1996). Experimental studies have also shown that angiogenic cytokines such as VEGF, aFGF, bFGF and angiogenin have a marked affinity for heparin and that these cytokines are likely to exist in bound form, as well as soluble form, in the extracellular matrix (D'Amore and Klagsbrun, 1984; Gospodarowicz *et al.*, 1984; Lobb and Fett, 1984; Maciag *et al.*, 1984; Sullivan and Klagsbrun, 1985). Taking these observations into account would involve modeling the distribution of heparin within the matrix and the subsequent binding of TAF to the heparin.

The technique of using partial differential equations as the basis for discrete models is clearly very useful, with the ability to generate movements of individual cells based on a continuum model of a population of cells. Indeed, this technique provides a powerful means of linking microscale events to macroscale

events and individual behaviour to population behaviour, with potential application to a wide range of problems in mathematical biology. Another advantage of using this technique is the possibility of manipulating the underlying spatial environment. For example, with respect to angiogenesis, the inclusion of an obstruction, such as a piece of cartilage, to block endothelial cell migration could easily be incorporated or the inclusion of an underlying spatially heterogeneous medium, which more faithfully reflects the make-up of an extracellular matrix, could also be incorporated. Such theoretical experiments are already in progress. The discrete model also offers a useful alternative to stochastic partial differential equations (cf. Stokes and Lauffenburger, 1991), combining, in an elegant and efficient way, the strengths of continuum models with the element of randomness.

Other important aspects of angiogenesis which can be added to the model in the future include incorporating blood flow through the capillary network (Muthukkarupann *et al.*, 1982), the role of oxygen gradients and oxygen concentration (Knighton *et al.*, 1981) and the role of macrophages (Polverini *et al.*, 1977; Knighton *et al.*, 1983; Lewis *et al.*, 1995). These aspects are also very important to angiogenesis in wound healing.

Finally, we note that antiangiogenesis strategies, such as the preferential killing of endothelial cells (Brooks *et al.*, 1994), the inhibition of endothelial-cell proliferation via a chemical such as angiostatin (O'Reilly *et al.*, 1994), the development of antichemotactic drugs (Bussolino *et al.*, 1992) and the development of antihaptotactic drugs (Yamada and Olden, 1978), are now clinically recognized as having enormous potential and promise in the treatment of patients with cancer (Harris, 1997). In particular, their use as an adjuvant chemotherapy is being recognized as a very effective way to treat secondary tumors (metastases), and mathematical models of angiogenesis may have an increasingly important role to play in the development and testing of these therapies.

ACKNOWLEDGEMENTS

MC thanks Professor Sean McElwain for helpful preliminary discussion concerning discrete modeling during a visit to Queensland University of Technology, August/September 1995, and thanks QUT and CiSSaIM for financial support. The authors thank Professor Seth Schor (Cell Biology) for a critical reading of the manuscript. This work was partly supported by BBSRC Grant MMI09008.

APPENDIX

To discretize the continuous system (8) we use Euler finite difference approximations (Mitchell and Griffiths, 1980), which leads to the system,

$$
\begin{aligned}
n_{l,m}^{q+1} &= n_{l,m}^{q} P_0 + n_{l+1,m}^{q} P_1 + n_{l-1,m}^{q} P_2 + n_{l,m+1}^{q} P_3 + n_{l,m-1}^{q} P_4, \\
f_{l,m}^{q+1} &= f_{l,m}^{q} \left[1 - k\gamma n_{l,m}^{q}\right] + k\beta n_{l,m}^{q}, \\
c_{l,m}^{q+1} &= c_{l,m}^{q} \left[1 - k\eta n_{l,m}^{q}\right],
\end{aligned}
$$

with $x = lh$, $y = mh$ and $t = pk$.

The coefficient P_0, which is proportional to the probability of no movement, has the form,

$$\begin{aligned} P_0 = 1 \quad & -\frac{4kD}{h^2} + \frac{k\alpha\chi(c^q_{l,m})}{4h^2(1+\alpha c^q_{l,m})}\left[\left(c^q_{l+1,m} - c^q_{l-1,m}\right)^2 + \left(c^q_{l,m+1} - c^q_{l,m-1}\right)^2\right] \\ & -\frac{k\chi(c^q_{l,m})}{h^2}\left(c^q_{l+1,m} + c^q_{l-1,m} - 4c^q_{l,m} + c^q_{l,m+1} + c^q_{l,m-1}\right) \\ & -\frac{k\rho}{h^2}\left(f^q_{l+1,m} + f^q_{l-1,m} - 4f^q_{l,m} + f^q_{l,m+1} + f^q_{l,m-1}\right), \end{aligned}$$

and the coefficients P_1, P_2, P_3 and P_4, which are proportional to the probabilities of moving left, right, up and down respectively, have the forms,

$$P_1 = \frac{kD}{h^2} - \frac{k}{4h^2}\left[\chi(c^q_{l,m})\left(c^q_{l+1,m} - c^q_{l-1,m}\right) + \rho\left(f^q_{l+1,m} - f^q_{l-1,m}\right)\right],$$

$$P_2 = \frac{kD}{h^2} + \frac{k}{4h^2}\left[\chi(c^q_{l,m})\left(c^q_{l+1,m} - c^q_{l-1,m}\right) + \rho\left(f^q_{l+1,m} - f^q_{l-1,m}\right)\right],$$

$$P_3 = \frac{kD}{h^2} - \frac{k}{4h^2}\left[\chi(c^q_{l,m})\left(c^q_{l,m+1} - c^q_{l,m-1}\right) + \rho\left(f^q_{l,m+1} - f^q_{l,m-1}\right)\right],$$

$$P_4 = \frac{kD}{h^2} + \frac{k}{4h^2}\left[\chi(c^q_{l,m})\left(c^q_{l,m+1} - c^q_{l,m-1}\right) + \rho\left(f^q_{l,m+1} - f^q_{l,m-1}\right)\right].$$

When there is no TAF or fibronectin in the same region as an endothelial cell, P_1–P_4 are equal since the values of c and f are 0. Also when there is an equal amount of TAF and fibronectin on either side of an endothelial cell (i.e., no gradient), the values $(c, f)_{l,m-1}$ and $(c, f)_{l,m+1}$ cancel each other out as do $(c, f)_{l-1,m}$ and $(c, f)_{l+1,m}$ and thus P_1–P_4 are equal. Therefore, in both these circumstances unbiased random movements will be produced. However, if there is more TAF (fibronectin) on one side of the endothelial cell than the other, the probabilities (P_1–P_4) will no longer be equal and hence directed movement towards the higher concentration of TAF (fibronectin), will result. If both TAF and fibronectin gradients exist then the probabilities will be biased by both gradients, depending on the coefficients χ and ρ.

REFERENCES

Alberts, B., D. Bray, J. Lewis, M. Raff, K. Roberts and J. D. Watson (1994). *The Molecular Biology of the Cell*, 3rd edn, New York: Garland Publishing.

Albini, A., G. Allavena, A. Melchiori, F. Giancotti, H. Richter, P. M. Comoglio, S. Parodi, G. R. Martin and G. Tarone (1987). Chemotaxis of 3T3 and SV3T3 cells to fibronectin is mediated through the cell-attachment site in fibronectin and fibronectin cell surface receptor. *J. Cell Biol.* **105**, 1867–1872.

Alessandri, G., K. S. Raju and P. M. Gullino (1986). Interaction of gangliosides with fibronectin in the mobilization of capillary endothelium. Possible influence on the growth of metastasis. *Invasion Metastasis* **6**, 145–165.

Alt, W. (1980). Biased random walk models for chemotaxis and related diffusion approximations. *J. Math. Biol.* **9**, 147–177.

Anderson, A. R. A. and M. A. J. Chaplain (1998). A mathematical model for capillary network formation in the absence of endothelial cell proliferation. *App. Math. Lett.* **11** (to appear).

Anderson, A. R. A., B. D. S. Sleeman, I. M. Young and B. S. Griffiths (1997). Nematode movement along a chemical gradient in a structurally heterogeneous environment: II. Theory. *Fundam. Appl. Nematol.* **20**, 165–172.

Arnold, F. and D. C. West (1991). Angiogenesis in wound healing. *Pharmac. Ther.* **52**, 407–422.

Ausprunk, D. H. and J. Folkman (1977). Migration and proliferation of endothelial cells in preformed and newly formed blood vessels during tumour angiogenesis. *Microvasc. Res.* **14**, 53–65.

Balding, D. and D. L. S. McElwain (1985). A mathematical model of tumour-induced capillary growth. *J. Theor. Biol.* **114**, 53–73.

Bell, A. D. (1986). The simulation of branching patterns in modular organisms. *Phil. Trans. Roy. Soc. Lond.* **B313**, 143–159.

Bell, A. D., D. Roberts and A. Smith (1979). Branching patterns: the simulation of plant architecture. *J. Theor. Biol.* **81**.

Ben-Zvi, A., M. M. Rodrigues, J. H. Krachmer and L. S. Fujikawa (1986). Immunohistochemical characterisation of extracellular matrix in the developing human cornea. *Curr. Eye Res.* **5**, 105–117.

Bikfalvi, A. (1995). Significance of angiogenesis in tumour progression and metastasis. *Eur. J. Cancer* **31A**, 1101–1104.

Birdwell, C. R., A. R. Brasier and L. A. Taylor (1980). Two-dimensional peptide mapping of fibronectins from bovine aortic endothelial cells and bovine plasma. *Biochem. Biophys. Res. Commun.* **97**, 574–581.

Birdwell, C. R., D. Gospodarowicz and G. L. Nicolson (1978). Identification, localisation and role of fibronectin in cultured endothelial cells. *Proc. Natl. Acad. Sci. USA* **75**, 3273–3277.

Bowersox, J. C. and N. Sorgente (1982). Chemotaxis of aortic endothelial cells in response to fibronectin. *Cancer Res.* **42**, 2547–2551.

Bray, D. (1992). *Cell Movements*, New York: Garland Publishing.

Brooks, P. C., A. M. P. Montgomery, M. Rosenfeld, R. A. Reisfled, T. Hu, G. Klier and D. A. Cheresh (1994). Integrin $\alpha_v\beta_3$ antagonists promote tumor regression by inducing apoptosis of angiogenic blood vessels. *Cell* **79**, 1157–1164.

Bussolino, F., M. F. Di Renzo, M. Ziche, E. Bocchietto, M. Olivero, L. Naldini, G. Gaudino, L. Tamagnone, A. Coffer and P. M. Comoglio (1992). Hepatocyte growth factor is a potent angiogenic factor which stimulates endothelial cell motility and growth. *J. Cell Biol.* **119**, 629–641.

Byrne, H. M. and M. A. J. Chaplain (1995). Mathematical models for tumour angiogenesis: numerical simulations and nonlinear wave solutions. *Bull. Math. Biol.* **57**, 461–486.

Carter, S. B. (1965). Principles of cell motility: the direction of cell movement and cancer invasion. *Nature* **208**, 1183–1187.

Carter, S. B. (1967). Haptotaxis and the mechanism of cell motility. *Nature* **213**, 256–260.

Chaplain, M. A. J. (1995). The mathematical modelling of tumour angiogenesis and invasion *Acta Biotheor.* **43**, 387–402.

Chaplain, M. A. J. (1996). Avascular growth, angiogenesis and vascular growth in solid

tumours: the mathematical modelling of the stages of tumour development. *Math. Comput. Model.* **23**, 47–87.

Chaplain, M. A. J. and A. M. Stuart (1993). A model mechanism for the chemotactic response of endothelial cells to tumour angiogenesis factor. *IMA J. Math. Appl. Med. Biol.* **10**, 149–168.

Clark, R. A. F., P. DellaPelle, E. Manseau, J. M. Lanigan, H. F. Dvorak and R. B. Colvin (1982). Blood vessel fibronectin increases in conjunction with endothelial cell proliferation and capillary ingrowth during wound healing. *J. Invest. Dermatol.* **79**, 269–276.

Clark, R. A. F, H. F. Dvorak and R. B. Colvin (1981). Fibronectin in delayed-type hypersensitivity skin reactions: associations with vessel permeability and endothelial cell activation. *J. Immunol.* **126**, 787–793.

Clark, R. A. F, H. J. Winn, H. F. Dvorak and R. B. Colvin (1983). Fibronectin beneath reepithelializing epidermis *in vivo*: sources and significance. *J. Invest. Dermatol.* **80**, 26–30.

Cliff, W. J. (1963). Observations on healing tissue: A combined light and electron microscopic investigation. *Trans. Roy. Soc. Lond.* **B246**, 305–325.

Dallon, J. C. and H. G. Othmer (1997). A discrete cell model with adaptive signalling for aggregation of *Dictyostelium discoideum*. *Phil. Trans. Roy. Soc. Lond.* **B352**, 391–417.

D'Amore, P. A. and M. Klagsbrun (1984). Endothelial cell mitogens derived from retina and hypothalamus—biochemical and biological similarities *J. Cell Biol.* **99**, 1545–1549.

Davis, B. (1990). Reinforced random walk. *Probab. Th. Rel. Fields* **84**, 203–229.

Deno, D. C., T. M. Saba and E. P. Lewis (1983). Kinetics of endogenously labeled plasma fibronectin: Incorporation into tissues. *Am. J. Physiol.* **245**, R564–R575.

Düchting, W. (1990a). Tumor growth simulation. *Comput. Graph.* **14**, 505–508.

Düchting, W. (1990b). Computer simulation in cancer research, in *Advanced Simulation in Biomedicine*, D. P. F. Möller (Ed.), pp. 117–139. New York: Springer-Verlag.

Düchting, W. (1992). Simulation of malignant cell growth, in *Fractal Geometry and Computer Graphics*, J. L. Encarnção, H. -O. Peitgen, G. Sakas and G. Englert (Eds), pp. 135–143. New York: Springer-Verlag.

Düchting, W., W. Ulmer and T. Ginsberg (1996). Cancer: A challenge for control theory and computer modelling. *Eur. J. Cancer* **32A**, 1283–1292.

Duh, E. J., G. L. King and L. P. Aiello (1997). Identification of a VEGF receptor (KDR/FLK) promoter element which binds an endothelial cell-specific protein conferring endothelial selective expression. *Invest. Opthamol. Vis. Sci.* **38**, 1124–1125.

Dumont, D. J., G. Gradwohl, G. H. Fong, M. C. Puri, M. Gertsenstein, A. Auerbach and M. L. Breitman (1994). Dominant-negative and targeted null mutations in the endothelial receptor tyrosine kinase, TEK, reveal a critical role in vasculogenesis of the embryo. *Genes Dev.* **8**, 1897–1909.

Edelstein-Keshet, L. and G. B Ermentrout (1989). Models for branching networks in two dimensions. *SIAM J. Appl. Math.* **49**, 1136–1157.

Ellis, L. E. and I. J. Fidler (1995). Angiogenesis and breast cancer metastasis. *Lancet* **346**, 388–389.

Ermentrout, G. B. and L. Edelstein-Keshet (1993). Cellular automata approaches to biological modelling. *J. Theor. Biol.* **160**, 97–133.

Folkman, J. (1985). Tumor angiogenesis. *Adv. Cancer Res.* **43**, 175–203.

Folkman, J. (1995). Angiogenesis in cancer, vascular, rheumatoid and other disease. *Nat.*

Med. **1**, 21–31.

Folkman, J. and H. Brem (1992). Angiogenesis and inflammation, in *Inflammation: Basic Principles and Clinical Correlates*, J. I. Gallin, I. M. Goldstein and R. Snyderman (Eds), 2nd edn, New York: Raven Press.

Folkman, J. and C. Haudenschild (1980). Angiogenesis *in vitro*. *Nature* **288**, 551–556.

Folkman, J. and M. Klagsbrun (1987). Angiogenic factors. *Science* **235**, 442–447.

Fong, G. H., J. Rossant, M. Gertsenstein and M. L. Breitman (1995). Role of the FLT-1 receptor tyrosine kinase in regulating the assembly of vascular endothelium. *Nature* **376**, 66–70.

Gasparini, G. (1995). Tumour angiogenesis as a prognostic assay for invasive ductal breast-carcinoma. *J. Natl. Cancer Inst.* **87**, 1799–1801.

Gasparini, G. and A. L. Harris (1995). Clinical importance of the determination of tumour angiogenesis in breast-cancer—much more than a new prognostic tool. *J. Clin. Oncol.* **13**, 765–782.

Gimbrone, M. A., R. S. Cotran, S. B. Leapman and J. Folkman (1974). Tumor growth and neovascularization: an experimental model using the rabbit cornea. *J. Natln. Cancer Inst.* **52**, 413–427.

Goodman, S. L. and D. Newgreen (1985). Do cells show an inverse locomotory response to fibronectin and laminin substrates? *EMBO J.* **4**, 2769–2771.

Gospodarowicz, D., J. Cheng, G. M. Lui, A. Baird and P. Bohlen (1984). Isolation of brain fibroblast growth-factor by heparin- sepharose affinity-chromatography—identity with pituitary fibroblast growth-factor. *Proc. Natl. Acad. Sci. USA* **81**, 6963–6967.

Gottlieb, M. E. (1990). Modelling blood vessels: a deterministic method with fractal structure based on physiological rules, in *Proc. 12th International Conference of IEEE EMBS*, pp. 1386–1387. New York: IEEE Press.

Gottlieb, M. E. (1991a). The VT model: a deterministic model of angiogenesis and biofractals based on physiological rules, in *Proc. IEEE 17th Annual Northeast Bioengineering Conference*, pp. 38–39. New York: IEEE Press.

Gottlieb, M. E. (1991b). Vascular networks: fractal anatomies from non-linear physiologies. *IEEE Eng. Med. Bio. Mag.* **13**, 2196–2197.

Graham, C. H. and P. K. Lala (1992). Mechanisms of placental invasion of the uterus and their control. *Biochem. Cell Biol.* **70**, 867–874.

Greenberg, J. H., S. Seppa, H. Seppa and A. T. Hewitt (1981). Role of collagen and fibronectin in neural crest cell adhesion and migration. *Dev. Biol.* **87**, 259–266.

Hanahan, D. (1997). Signaling vascular morphogenesis and maintenance. *Science* **227**, 48–50.

Harris, A. L. (1997). Antiangiogenesis for cancer therapy. *Lancet* **349** (suppl. II), 13–15.

Harris, A. L., S. Fox, R. Bicknell, R. Leek and K. Gatter (1994). Tumour angiogenesis in breast-cancer—prognostic factor and therapeutic target. *J. Cellular Biochem.* **S18D SID**, 225.

Harris, A. L., H. T. Zhang, A. Moghaddam, S. Fox, P. Scott, A. Pattison, K. Gatter, I. Stratford and R. Bicknell (1996). Breast cancer angiogenesis—new approaches to therapy via anti- angiogenesis, hypoxic activated drugs, and vascular targeting. *Breast Cancer Res. Treat.* **38**, 97–108.

Hatva, E., A. Kaipainen, P. Mentula, J. Jaaskelainen, A. Paetau, M. Haltia and K. Alitalo (1995). Expression of endothelial cell-specific receptor tyrosine kinases and growth-factors in human brain-tumors. *Am. J. Pathol.* **146**, 368–378.

Herblin, W. F. and J. L. Gross (1994). Inhibition of angiogenesis as a strategy for tumour-

growth control. *Mol. Chem. Neuropath.* **21**, 329–336.
Hewett, P. W. and J. C. Murray (1996). Coexpression of FLT-1, FLT-4 and KDR in freshly isolated and cultured human endothelial-cells. *Biochem. Biophys. Res. Commun.* **221**, 697–702.
Höfer, T., J. A. Sherratt and P. K. Maini (1995). Cellular pattern formation during *Dictyostelium* aggregation. *Physica* **D85**, 425–444.
Hynes, R. O. (1990). *Fibronectins*, Springer-Verlag: New York.
Indermitte, C., Th. M. Liebling and H. Clémonçon (1994). Culture analysis and external interaction models of mycelial growth. *Bull. Math. Biol.* **56**, 633–664.
Jaffee, E. A. and D. F. Mosher (1978). Synthesis of fibronectin by cultured endothelial cells. *J. Exp. Med.* **147**, 1779–1791.
Johansson, S., S. Gustafson and H. Pertoft (1987). Identification of a fibronectin receptor specific for rat liver endothelial cells. *Exp. Cell Res.* **172**, 425–431.
Kiani, M. and A. Hudetz (1991). Computer simulation of growth of anastomosing microvascular networks. *J. Theor. Biol.* **150**, 547–560.
Knighton, D. M., T. K. Hunt, H. Scheuenstuhl and B. J. Halliday (1983). Oxygen tension regulates the expression of angiogenesis factor by macrophages. *Science* **221**, 1283–1285.
Knighton, D. M., I. A. Silver and T. K. Hunt (1981). Regulation of wound-healing angiogenesis—effect of oxygen gradients and inspired oxygen concentration. *Surgery* **90**, 262–270.
Kohno, T., N. Sorgente, T. Ishibashi, R. Goodnight and S. J. Ryan (1987). Immunofluorescent studies of fibronectin and laminin in the human eye. *Invest. Opthamol. Vis. Sci.* **28**, 506–514.
Kohno, T., N. Sorgente, R. Patterson and S. J. Ryan (1983). Fibronectin and laminin distribution in bovine eye. *Jpn. J. Opthamol.* **27**, 496–505.
Lacovara, J., E. B. Cramer and J. P. Quigley (1984). Fibronectin enhancement of directed migration of B16 melanoma cells. *Cancer Res.* **44**, 1657–1663.
Landini, G. and G. Misson (1993). Simulation of corneal neo–vascularization by inverted diffusion limited aggregation. *Invest. Opthamol. Visual Sci.* **34**, 1872–1875.
Lapidus, I. R. and R. Schiller (1976). Model for the chemotactic response of a bacterial population. *Biophys. J.* **16**, 779–789.
Lauffenburger, D., R. Aris and C. R. Kennedy (1984). Travelling bands of chemotactic bacteria in the context of population growth. *Bull. Math. Biol.* **46**, 19–40.
Lewis, C. E., R. Leek, A. Harris and J. O. D. McGee (1995). Cytokine regulation of angiogenesis in breast-cancer—the role of tumour-associated macrophages. *J. Leukocyte Biol.* **57**, 747–751.
Lewis, J., J. M. W. Slack and L. Wolpert (1977). Thresholds in development. *J. Theor. Biol.* **65**, 579–590.
Liotta, L. A., C. N. Rao and S. H. Barsky (1983). Tumour invasion and the extracellular matrix. *Lab. Invest.* **49**, 636–649.
Liotta, L. A., G. M. Saidel and J. Kleinerman (1977). Diffusion model of tumor vascularization. *Bull. Math. Biol.* **39**, 117–128.
Lobb, R. R. and J. W. Fett (1984). Purification of two distinct growth-factors from bovine neural tissue by heparin affinity-chromatography. *Biochemistry* **23**, 6295–6299.
McCarthy, J. B. and L. T. Furcht (1984). Laminin and fibronectin promote the directed migration of B16 melanoma cells *in vitro*. *J. Cell Biol.* **98**, 1474–1480.
Macarak, E. J., E. Kirby, T. Kirk and N. A. Kefalides (1978). Synthesis of cold-insoluble

globulin cultured by calf endothelial cells. *Proc. Natl. Acad. Sci. USA* **75**, 2621–2625.

Maciag, T., T. Mehlman, R. Friesel and A. B. Schreiber (1984). Heparin binds endothelial cell-growth factor, the principal endothelial cell mitogen in bovine brain. *Science* **225**, 932–935.

Madri, J. A. and B. M. Pratt (1986). Endothelial cell-matrix interactions: *in vitro* models of angiogenesis. *J. Histochem. Cytochem.* **34**, 85–91.

Mandriota, S. J., G. Seghezzi, J. D. Vassalli, N. Ferrara, S. Wasi, R. Mazzieri, P. Mignatti and M. S. Pepper (1995). Vascular endothelial growth-factor increases urokinase receptor expression in vascular endothelial-cells. *J. Biol. Chem.* **270**, 9709–9716.

Meinhardt, H. (1976). Morphogenesis of lines and nets. *Differentiation* **6**, 117–123.

Meinhardt, H. (1982). *Models of Biological Pattern Formation*, London: Academic Press.

Millauer, B., Wizigman-Voos, H. Schnürch, R. Martinez, N. P. H. Müller, W. Risau and A. Ullrich (1993). High-affinity VEGF binding and developmental expression suggest FLK-1 as a major regulator of vasculogenesis and angiogenesis. *Cell* **72**, 835–846.

Mitchell, A. R. and D. F. Griffiths (1980). *The Finite Difference Method in Partial Differential Equations*, Chichester: Wiley.

Monaghan, P., M. J. Warburton, N. Perusinghe and P. S. Rutland (1983). Topographical arrangement of basement membrane proteins in lactating rat mammary gland: comparison of the distribution of Type IV collagen, laminin, fibronectin and Thy-1 at the ultrasructural level. *Proc. Natl. Acad. Sci.* **80**, 3344–3348.

Muthukkaruppan, V. R., L. Kubai and R. Auerbach (1982). Tumor-induced neovascularization in the mouse eye. *J. Natl. Cancer Inst.* **69**, 699–705.

Nekka, F., S. Kyriacos, C. Kerrigan and L. Cartilier (1996). A model of growing vascular structures. *Bull. Math. Biol.* **58**, 409–424.

Norton, J. A. (1995). Tumor angiogenesis: the future is now. *Ann. Surg.* **222**, 693–694.

Oh, E., M. Pierschbacher and E. Ruoslahti (1981). Deposition of plasma fibronectin in tissues. *Proc. Natl. Acad. Sci. USA* **78**, 3218–3221.

Olsen, L., J. A. Sherratt, P. K. Maini and F. Arnold (1997). A mathematical model for the capillary endothelial cell-extracellular matrix interactions in wound-healing angiogenesis. *IMA J. Math. Appl. Med. Biol.* **14**, 261–281.

O'Reilly, M. S., L. Holmgren, Y. Shing, C. Chen, R. A. Rosenthal, M. Moses, W. S. Lane, Y. Cao, E. Helene Sage and J. Folkman (1994). Angiostatin: a novel angiogenesis inhibitor that mediates the suppression of metastases by a Lewis lung carcinoma. *Cell* **79**, 315–328.

Orme, M. E. and M. A. J. Chaplain (1996). A mathematical model of the first steps of tumour-related angiogenesis: capillary sprout formation and secondary branching. *IMA J. Math. App. Med. and Biol.* **13**, 73–98.

Orme, M. E. and M. A. J. Chaplain (1997). Two-dimensional models of tumour angiogenesis and anti-angiogenesis strategies. *IMA J. Math. App. Med. and Biol.* **14**, 189–205.

Ortega, N., D. Dossantos and J. Plouet (1996). Activation of the VEGF receptor FLT-1 mediates corneal endothelial-cell migration permeability. *Invest. Optham. Vis. Sci.* **37**, 417–418.

Ortega, N. and J. Plouet (1995). Constitutive expression of the VEGF receptor KDR/FLK-1 in corneal endothelial-cell mediates their proliferation. *Vis. Res.* **35**, 4217–4218.

Othmer, H. and A. Stevens (1997). Aggregation, blowup and collapse: The ABCs of taxis and reinforced random walks. *SIAM J. Appl. Math.* **57** 1044–1081.

Paku, S. and N. Paweletz (1991). First steps of tumor-related angiogenesis. *Lab. Invest.* **65**, 334–346.

Patterson, C., M. A. Perrella, W. O. Endege, M. Yoshizumi, M. E. Lee and E. Haber (1996). Down-regulation of vascular endothelial growth- factor receptors by tumor-necrosis-factor-alpha in cultured human vascular endothelial-cells. *J. Clin. Invest.* **98**, 490–496.

Paweletz, N. and M. Knierim (1989). Tumor-related angiogenesis. *Crit. Rev. Oncol. Hematol.* **9**, 197–242.

Pettet, G., M. A. J. Chaplain, D. L. S. McElwain and H. M. Byrne (1996). On the role of angiogenesis in wound healing. *Proc. Roy. Soc. Lond.* **B263**, 1487–1493.

Polverini, P. J., R. S. Cotran, M. A. Gimbrone Jr. and E. R. Unanue (1977). Activated macrophages induce vascular proliferation. *Nature* **269**, 804–806.

Prusinkiewicz, P. and A. Lindenmayer (1990). *The Algorithmic Beauty of Plants*, New York: Springer-Verlag.

Quigley, J. P., J. Lacovara and E. B. Cramer (1983). The directed migration of B-16 melanoma-cells in response to a haptotactic chemotactic gradient of fibronectin. *J. Cell Biol.* **97**, A450–451.

Relf, M., S. Lejeune, P. A. E. Scott, S. Fox, K. Smith, R. Leek, A. Mogaddam, R. Whitehouse, R. Bicknell and A. L. Harris (1997). Expression of the angiogenic factors vascular endothelial cell growth factor, acidic and basic fibroblast growth factor, tumour growth factor beta-1, platelet-derived endothelial cell growth factor, placenta growth factor and pleiotrophin in human primary breast cancer and its relation to angiogenesis. *Cancer Res.* **57**, 963–969.

Rieder, H., G. Ramadori, H. P. Dienes and K. H. Meyer zum Buschenfelde (1987). Sinusoidal endothelial cells from guinea pig liver synthesize and secrete cellular fibronectin *in vitro*. *Hepatology* **7**, 856–864.

Rocco, M., E. Infusini, M. G. Daga, L. Gogioso and C. Cuniberti (1987). Models of fibronectin. *EMBO J.* **6**, 2343–2349.

Rupnick, M. A., C. L. Stokes, S. K. Williams and D. A. Lauffenburger (1988). Quantitative analysis of human microvessel endothelial cells using a linear under-agarose assay. *Lab. Invest.* **59**, 363–372.

Sato, T. N., Y. Tozawa, U. Deutsch, K. Wolburgbuchholz, Y. Fujiwara, M. Gendron-maguire, T. Gridley, H. Wolburg, W. Risau and Y. Qin (1995). Distinct roles of the receptor tyrosine kinases TIE-1 and TIE-2 in blood-vessel formation. *Nature* **376**, 70–74.

Sawada, H., H. Furthmayr, H. Konomi and Y. Nagai (1987). Immunoelectronmicroscopic localization of extracellular matrix components produced by bovine corneal endothelial cells *in vitro*. *Exp. Cell Res.* **171**, 94–109.

Schoefl, G. I. (1963). Studies on inflammation III. Growing capillaries: Their structure and permeability. *Virchows Arch. Pathol. Anat.* **337**, 97–141.

Schor, S. L., A. M. Schor and G. W. Brazill (1981). The effects of fibronectin on the migration of human foreskin fibroblasts and syrian hamster melanoma cells into three-dimensional gels of lattice collagen fibres. *J. Cell Sci.* **48**, 301–314.

Sherratt, J. A. (1994). Chemotaxis and chemokinesis in eukaryotic cells: The Keller–Segel equations as an approximation to a detailed model. *Bull. Math. Biol.* **56**, 129–146.

Sherratt, J. A. and J. D. Murray (1990). Models of epidermal wound healing. *Proc. Roy. Soc. Lond.* **B241**, 29–36.

Sherratt, J. A., E. H. Sage and J. D. Murray (1993). Chemical control of eukaryotic cell movement: a new model. *J. Theor. Biol.* **162**, 23–40.

Sholley, M. M., G. P. Ferguson, H. R. Seibel, J. L. Montour and J. D. Wilson (1984).

Mechanisms of neovascularization. Vascular sprouting can occur without proliferation of endothelial cells. *Lab. Invest.* **51**, 624–634.

Sramek, S. J., I. H. Wallow, C. Bindley and G. Sterken (1987). Fibronectin distribution in the rat eye. An immunohistochemical study. *Invest. Opthamol. Vis. Sci.* **28**, 500–505.

Stokes, C. L. and D. A. Lauffenburger (1991). Analysis of the roles of microvessel endothelial cell random motility and chemotaxis in angiogenesis. *J. Theor. Biol.* **152**, 377–403.

Stokes, C. L., M. A. Rupnick, S. K. Williams and D. A. Lauffenburger (1990). Chemotaxis of human microvessel endothelial cells in response to acidic fibroblast growth factor. *Lab. Invest.* **63**, 657–668.

Stokes, C. L., D. A. Lauffenburger and S. K. Williams (1991). Migration of individual microvessel endothelial cells: stochastic model and parameter measurement *J. Cell Sci.* **99**, 419–430.

Sullivan, R. and M. Klagsbrun (1985). Purification of cartilage-derived growth-factor by heparin affinity-chromatography. *J. Biol. Chem.* **260**, 2399–2403.

Terranova, V. P., R. Diflorio, R. M. Lyall, S. Hic, R. Friesel and T. Maciag (1985). Human endothelial cells are chemotactic to endothelial cell growth factor and heparin. *J. Cell Biol.* **101**, 2330–2334.

Vlodavsky, I., L. K. Johnson, G. Greenburg and D. Gospodarowicz (1979). Vascular endothelial cells maintained in the absence of fibroblast growth factor undergo structural and functional alterations that are incompatible with their *in vivo* differentiated properties. *J. Cell Biol.* **83**, 468–486.

Warren, B. A. (1966). The growth of the blood supply to melanoma transplants in the hamster cheek pouch. *Lab. Invest.* **15**, 464–473.

Weimar, J. R., J. J. Tyson and L. T. Watson (1992a). Diffusion and wave-propagation in cellular automaton models of excitable media. *Physica* **D55**, 309–327.

Weimar, J. R., J. J. Tyson and L. T. Watson (1992b). 3rd generation cellular automaton for modelling excitable media. *Physica* **D55**, 327–339.

Williams, E. C., P. A. Janmey, J. D. Ferry and D. F. Mosher (1982). Conformational states of fibronectin. Effects of pH, ionic strength and collagen–binding. *J. Biol. Chem.* **257**, 14973–14978.

Williams, S. K. (1987). Isolation and culture of microvessel and large-vessel endothelial cells; their use in transport and clinical studies, in *Microvascular Perfusion and Transport in Health and Disease*, P. McDonagh (Ed.), pp. 204–245. Basel: Karger.

Wolpert, L. (1981). Positional information and pattern formation. *Phil. Trans. Roy. Soc. Lond.* **B295**, 441–450.

Woodley, D. T., P. M. Bachmann and E. J. O'Keefe (1988). Laminin inhibits human keratinocyte migration. *J. Cell Physiol.* **136**, 140–146.

Woodward, D. E., R. Tyson, M. R. Myerscough, J. D. Murray, E. O. Budrene and H. C. Berg (1995). Spatio-temporal patterns generated by *Salmonella typhimurium*. *Biophys. J.* **68**, 2181–2189.

Yamada, K. M. and K. Olden (1978). Fibronectin-adhesive glycoproteins of cell surface and blood. *Nature* **275**, 179–184.

Zawicki, D. F., R. K. Jain, G. W. Schmid-Schoenbein and S. Chien (1981). Dynamics of neovascularization in normal tissue. *Microvasc. Res.* **21**, 27–47.

Received 23 March 1997 and accepted 15 January 1998